Universitat Autònoma de Barcelona

A Thesis for the

Master in Telecommunication Engineering

Analysis of RF-Energy Transducer for Microwave Harvesting System Suitable for IoT applications

by

Ariadna Sendra i Munita

Supervisor: Joan J. Garcia Garcia

Grup d'Aplicacions Electro-Magnètiques Industrials (GAEMI)
Departament d'Enginyeria Electrònica

Escola d'Enginyeria
Universitat Autònoma de Barcelona (UAB)

January 2020

El sotasignant, *Joan J. Garcia Garcia*, Professor de l'Escola d'Enginyeria de la Universitat Autònoma de Barcelona (UAB),

FA CONSTAR:

Que el projecte presentat en aquesta memòria de Treball Final de Màster ha estat realitzat sota la seva direcció per l'alumne *Ariadna Sendra i Munita*.

I, perquè consti a tots els efectes, signa el present certificat.

Bellaterra, *24 de Gener del 2020.*

Signatura: *Joan J. Garcia Garcia*

Resum:

Aquest projecte analitza numèricament la millora en eficiència dels elements del transductor d'energia de RF d'antenes confinades en cavitats metàl·liques. Per fer-ho, es realitzen estudis paramètrics mitjançant el simulador electromagnètic 3D CST dels transductors de RF proposats utilitzant dues antenes duals a 2.4/5 GHz i una patch-antenna dissenyada a 2.4 GHz. Els resultats obtinguts es contrasten amb mesures experimentals, arribant a demostrar que els transductors proposats generen prou potència per a alimentar un sistema de gestió d'energia basat en el xip comercial BQ25570 de Texas Instruments o alimentar sistemes IoT amb consums en el rang del µW.

Resumen:

El presente proyecto analiza numéricamente el aumento en eficiencia de los elementos del transductor de energía de RF de antenas confinadas en cavidades metálicas. Para ello, se realiza un estudio paramétrico mediante el simulador electromagnético 3D CST de los transductores de RF propuestos para dos antenas dipolos comerciales duales a 2.4/5 GHz y una patch antena diseñada a 2.4 GHz. Los resultados de las simulaciones se contrastan con medidas experimentales, llegando a demostrar que el transductor propuesto genera suficiente energía como para alimentar un sistema de gestión de energía estándar basado en el chip comercial BQ25570 de Texas Instruments o alimentar sistemas IoT con consumos en el rango de los µW.

Summary:

This project examines numerically the improved efficiency of energy transducer elements as RF antennas confined in metal cavities. To do so, parametric studies are performed using the 3D electromagnetic simulator CST transducers proposed using two RF antennas dual 2.4/5 GHz antenna and a patch-designed 2.4 GHz. The results are contrasted with experimental measurements, demonstrating that the proposed transducers generate enough power to power a Texas Instruments BQ25570 chip or power IoT systems with µW power consumption.

CONTENTS

1 Introduction 1

1.1 Motivation: how to improve the RF harvesting systems 1

1.2 State of art: current standards and open problems in antennas as RF energy transducers 2

1.3 IEEE 802.11 6

1.4 Objectives 8

2 CST Microwave Studio (CST MWS) 10

3 Working conditions 12

4 RF Antenna 15

4.1 Microstrip patch antenna 15

4.2 Patch antenna design and simulation 17

4.2.1 Design of a patch antenna 17

4.2.2 Simulation of the patch antenna 20

4.3 Dipole antennas 26

4.4 Dipole antennas structure description, experimental measurements and simulation 26

4.4.1 Structure description of the dipole antennas 27

4.4.2 Experimental measurements and simulation of the dipole antennas 31

5 Enhanced RF transducer 40

5.1 Measurement for experimental measurement set-up 40

5.2 Simulated behaviour 43

5.2.1 Metal layers sizes 44

5.2.2 Gap between the metal layers 48

6 Efficiency and application of the enhanced RF transducer 50

6.1 Efficiency 50

6.2 Combination of the enhanced transducer with the BQ25570 based energy management system 51
6.3 Harvest-1 and Harvest-2 52
7 Conclusions and future work 55
7.1 Conclusions 55
7.2 Future work 56
8 References 58
9 Annexes 61
9.1 Electrical features of the energy management system 61
9.2 Schematic of the energy management system 63
9.3 Electronic components of the energy management devices 64
9.4 CST far-field source file 65

LIST OF FIGURES

Figure 1-1. Schematic of RF energy harvesting system 2
Figure 1-2. Effect of highly non-linear rectification stage in a 2.4 GHz signal. a) Full-Wave Rectifier b) Measured amplitude in dBm of the input signal. c) Measured Amplitude in dBm of the output rectified signal [11] 3
Figure 1-3. Spectral density by the antenna and rectenna [11] 4
Figure 1-4. Scheme of RF-Energy Transducer: a standard antenna confined between the Fabry-Perot Cavity by metallic layers separated by a distance (GAP) around 0.1 mm. The output of the antenna is connected to a four Schottky diode rectifier bridge through a 50 UFL coaxial bridge [11] 4
Figure 1-5. Spectrum power density of an enhanced rectenna and non-enhanced rectenna [11] 5
Figure 1-6. Performance comparison between the RF collector with a free antenna and with the Fabry-Perot cavity by a 4-wire set up using a N6705C DC Power Analyzer [13] with two N6781A modules [14] 6
Figure 2-1. CST STUDIO SUITE modules 10
Figure 3-1. Power spectral density for the 47950-0001 Molex Combo antenna 12
Figure 3-2. Maximum available ambient power for the 47950-0001 Molex Combo antenna 13
Figure 4-1. Microstrip antenna: metal patch on top of a grounded dielectric substrate . 15
Figure 4-2. The different feeding methods with their equivalent circuits for microstrip antennas. a) Inset-fed. b) Patch proximity coupled to a microstrip feed line. c) Patch aperture coupled to a microstrip feed line [27] 17
Figure 4-3. Top view of rectangular microstrip feed line (inset-fed) 18
Figure 4-4. Impedance Calculation tool into CST 19
Figure 4-5. Model of the inset-fed patch antenna for a finite substrate (Rogers RO3010) 20
Figure 4-6. Reflection coefficient of the inset-fed patch antenna for a L parameter designed and L adjusted 21
Figure 4-7. Propagation modes of the inset-fed patch antenna 22
Figure 4-8. Reflection coefficient for a feeding point in W/2 and two different L positions: L default and L*0.3 23

Figure 4-9. Smith chart of the inset-fed patch antenna for L=19.07 mm 24
Figure 4-10. Current density of the inset-fed patch antenna at 2.4 GHz 24
Figure 4-11. Radiation pattern at 2.4 GHz in inset-fed patch antenna 25
Figure 4-12. E-field distribution of the inset-fed antenna at 2.4 GHz 25
Figure 4-13. Half-wave dipole antenna 26
Figure 4-14. Layout of Molex Combo antenna 47950-0001, where the orange area corresponds with the dielectric layer and the grey area with the substrate 27
Figure 4-15. Dimensions of the geometry of the Molex Combo antenna 47950-0001, where the orange area corresponds with the dielectric layer and the grey area with the substrate layer 27
Figure 4-16. Layout of Molex Combo antenna 47950-0011, where the orange area corresponds with the dielectric layer and the grey area with the substrate layer 28
Figure 4-17. Dimensions of the geometry of the Molex Combo antenna 47950-0011, where the orange area corresponds with the dielectric layer and the grey area with the substrate layer 28
Figure 4-18. Layers of the Molex Combo antennas. Polyimide substrate (grey) and copper metal layer (orange) separate by a gap of 0.2 mm 29
Figure 4-19. Measurement set-up using a Microscope Leica M80 [28]. a) Configuration calibration for x1.25 augment. b) Example of the measurement of the Molex Combo antenna 479500001 for x0.75 augment 30
Figure 4-20. Measure of the dipole antenna with the VNA. a) View of the adapters and connexions of the dipole antenna. b) Example about the S_{11} parameter measured 32
Figure 4-21. Reflection coefficient for the antenna 47950-0001 32
Figure 4-22. Reflection coefficient for the antenna 47950-0001 at 3, 3.5 and 4 to the dielectric constant 33
Figure 4-23. Reflection coefficient simulated and measured for the antenna 47950-0001 with a mesh refine 34
Figure 4-24. Reflection coefficient simulated and measured for the antenna 47950-00011 34
Figure 4-25. Smith chart of the antenna 47950-0001 35
Figure 4-26. Smith chart of the antenna 47950-0011 35
Figure 4-27. Current distributions for antenna 47950-0001 at 2.7 GHz a) and 5.5 GHz b). 36

Figure 4-28. Current distributions for antenna 47950-0011 at 2.8 GHz a) and 5.7 GHz b). 37
Figure 4-29. Radiation pattern for the antennas 47950-0001 and 47950-0011..... 38
Figure 4-30. E-field distribution in YX axis at 2.4 GHz for the antenna 47950-0001 a) and 47950-0011 b)..... 39
Figure 5-1. Different metal surfaces of FR4 with 35 µm of thickness..... 40
Figure 5-2. Experimental configuration with 4-wires connection between the RF transducer and DC Power Analyzer N6705C [13] by two modules N6781A [14]. a) The non-enhanced RF transducer is hold by a support for orientate of the RF signal in direction of the router. b) The enhanced RF transducer is between two metal layers with the antenna by a support for orientate of the RF signal in direction of the router..... 41
Figure 5-3. Output voltage of the enhanced RF transducer with a super-capacitance of 22 mF, for the Molex Combo antenna 47950-0001 and for different metallic surfaces by a measurement of 4-wire set up using a N6705C DC Power Analyzer [13] with two N6781A modules [14]..... 42
Figure 5-4. Output voltage of the enhanced RF transducer with a super-capacitance of 22 mF, for a Molex Combo antenna 47950-0001 and for different metallic surfaces by a measurement of 4-wire set up using a N6705C DC Power Analyzer [13] with two N6781A modules [14]..... 43
Figure 5-5. Schematic of enhanced RF transducer (left) for a far-field source (right) with a distance from the center of the antenna of 200 mm..... 44
Figure 5-6. E-field distribution at 2.4 GHz along XY-plane for Z=0 mm of the far-field source emitting in the left side. For the non-enhanced transducer a) and for the enhanced-transducer with gap=1 mm by Molex Combo 47950-0001 and metal layers of: 80x100 mm b), 150x200 mm c) and 200x300 mm d)..... 45
Figure 5-7. E-field distribution at 2.4 GHz along XY-plane for Z=0 mm of the far-field source emitting in the left side for the enhanced-transducer by Molex Combo 47950-0001 and metal layer 150x200 mm with gap=0.5 mm..... 46
Figure 5-8. E-field distribution along XY-plane at Z=0 mm of the Molex Combo antenna 47950-0001 into the resonant cavity 150x200 mm at 2.4 GHz with a gap=1 mm..... 46
Figure 5-9. E-field distribution at 2.4 GHz along XY-plane for Z=0 mm of the far-field source emitting in the left side for the enhanced-transducer by Molex Combo antenna 47950-0011 with a gap=1 mm and metal layers 151x206.9 mm a) and at top side for the inset-fed patch antenna with a gap=1 mm and metal layers 167.92x229.14 mm b)..... 47

Figure 5-10. Reflection coefficient of the enhanced RF transducer for Molex Combo antenna 47950-0001 with a gap of 20 mm, 50 mm and 100 mm 48
Figure 5-11. E-field distribution at 2.7 GHz: of the enhanced RF transducer for Molex Combo 47950-0001, metal surface of 150x200 mm with a gap of 24 mm a) and 20 mm b) 49
Figure 6-1. Evaluation module BQ25570EVM-206 by BQ25570 IC from Texas Instrument [12] 51
Figure 6-2. Output and input voltage of the step-up stage for the evaluation module BQ25570EVM-206 by BQ25570 IC from Texas Instrument [12]. The input voltage is provided of the enhanced RF transducer for a Molex Combo antenna 47950-0001 with a resonant cavity of 200x150 mm and a super-capacitance of 22 mF 52
Figure 6-3. Layout of Harvest-1 53
Figure 6-4. Output and input voltage of the step-up stage for the Harvest-1 by GAEMI group of UAB. The input voltage is provided of the enhanced RF transducer for a Molex Combo antenna 47950-0001 [7]with a resonant cavity of 200x150 mm and a super-capacitance of 22 mF 53
Figure 6-5. Layout of the Harvest-2 54
Figure 9-1. Short-circuit of the BQ25570EVM-206 between V_{BAT} and V_{STOR} 62

LIST OF TABLES

Table 1-1. Typical electronic devices consumption [2] 1
Table 1-2. IEEE 802.11 standards development history in reference to frequency bands, bandwidth and maximum data rate 7
Table 1-3. Distribution of the channels into 2.4 GHz band [16] 7
Table 3-1. Different services of communications [20] 13
Table 3-2. Channels into working conditions at 2.4 GHz 14
Table 4-1. Parameters design of the microstrip antenna 20
Table 4-2. TM modes of the inset-fed patch antenna 22
Table 4-3. Electrical specifications of the two models Molex Combo antennas [7], [8] 30
Table 4-4. Parameters design of the Molex Combo antennas 31
Table 4-5. Frequency resonances of the antenna 47950-0001 and 47950-0011 35

Table 6-1. Enhanced RF transducer efficiency for a different sizes of metal surfaces. The P_{DC} is measured at Δt=15 minutes for a super-capacitance of 22 mF. And the P_{RF} at 5 GHz 50
Table 9-1. Electrical features of the step-up stage..... 61

1 INTRODUCTION

1.1 MOTIVATION: HOW TO IMPROVE THE RF HARVESTING SYSTEMS

The Internet of Things (IoT) systems are grow up exponentially to recollect information from a multiply environment sources such as vibrations, sound, pressure or light increasing the use of Wireless Sensor Networks (WSNs). The WSN are defined as a network of devices (e.g. mobile phones or also autonomous sensors) capable of communicate data through multiple nodes, each network node is built by a radio transceiver with an antenna, a microcontroller, an electronic circuit for interfacing with the sensors and an energy source [1]. Consequently, the use of sensors into devices requires energy and cause a decreasing of the lifetime of the systems. To solve this drawback, this work proposes a harvesting system to feed and reduce the energy waste, transforming a small amount of radio frequency (RF) energy into an electric current able to feed WSN devices which require low power density in range of µW to mW (as can be observed in Table 1-1 [2]).

Power	**1 µW**	**10 µW**	**100 µW**	**1 mW**
Device	32 kHz Quartz oscillator	Watch, Calculator, Passive RFID	Hearing Aid, Temperature sensor	Active RFID, Miniature FM receiver

Table 1-1. Typical electronic devices consumption [2]

The most common harvesting systems are thermoelectric, piezoelectric, electrodynamic or photovoltaic, but one of the alternatives of power source is the far-field RF energy taking advantage for the rising amount of propagated wireless power in indoor-outdoor environment. The far-field RF energy harvesting system is based on a receiving antenna which provides consistent and predictable power at very low power density since the propagation energy drops off quickly as distance from the source is increased [3]. An example of the main sources of RF signals are transmitter antennas and towers, Wi-Fi routers, cellular networks, televisions transmitter and others [4] where there are works explain and shows the efficiency based on the density levels founded in an urban ambient [5] or also based on the density levels in function of the distance of the source to feed a WSN [3].

The present project is focused on the Wi-Fi source at 2.4 GHz for the proposed RF transducer. However, the described techniques are also suitable to extract energy from other RF sources in the range up to 6 GHz.

1.2 STATE OF ART: CURRENT STANDARDS AND OPEN PROBLEMS IN ANTENNAS AS RF ENERGY TRANSDUCERS

The basic principle of the proposed RF transducer (see Figure 1-1) is reuse part of the Wi-Fi energy waves emissions which is captured by an antenna and a transform it into a low power (typically in the μW range) direct current.

To accomplish it, once the energy is captured by an antenna pass for the AC to DC stage though a full-wave rectifier (diodes bridge). Then, the direct current DC is managed to be used by a step-up or energy management stage [6] and so storage the collected load with a super-capacity (SPC), an electrochemical device capable of storing more charge than a conventional capacitor, with low losses level and fast response (in range of GHz).

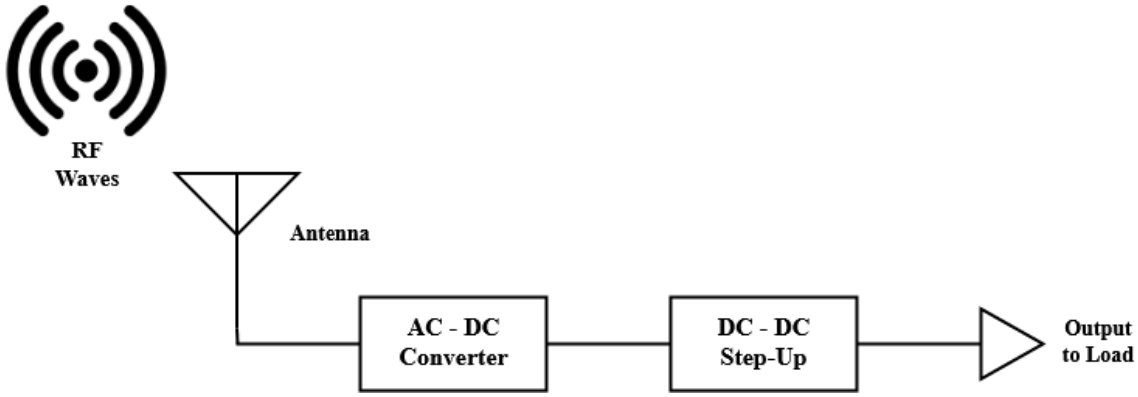

Figure 1-1. Schematic of RF energy harvesting system

The received and expected power of the Wi-Fi waves by the antenna is very small, therefore an antenna with a high gain is necessary to obtain greater power at the input of our circuit. For this reason, are chosen two models of dipoles antennas (Molex Combo 47950-0001 [7] and 47950-0011 [8]) to works at 2.4/5 GHz with an impedance of 50 Ω and peak gain of 2.27 dBi and 3 dBi in case of the second model.

For the AC to DC conversion stage, the input impedance should be agreed with the antenna to maximize the power transfer. A good alternative for an efficient system is a full-wave rectifier stage which is intrinsically a highly non-linear circuit due to the low threshold voltage (typically V_γ=150 mV) and its high response speed, useful for rectify

high frequency signals like the Wi-Fi waves [9]. The full-wave rectifier consist of four Schottky diodes (SMS7630 [10]) like the Figure 1-2.a) suppling charge to a super-capacitor of 8 mF.

See the behaviour non-linear for a monotone wave spectrum at 2.4 GHz (Figure 1-2.b)) before and after the rectification (Figure 1-2.c)), which there are some harmonic components at lower frequencies of 1 GHz and also around 2.4 GHz and 5 GHz. This fact implies some power lost in case of the best impedance matching to one single resonant frequency due to will acts as a filter for the rest of the spectrum power and is proposed an alternative of optimization based on a resonant cavity explained later.

a)

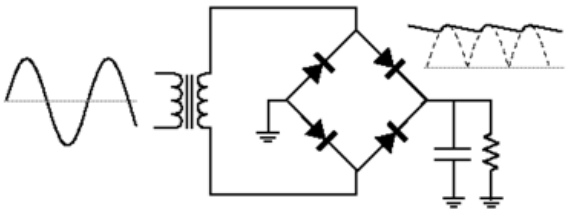

b)

c)

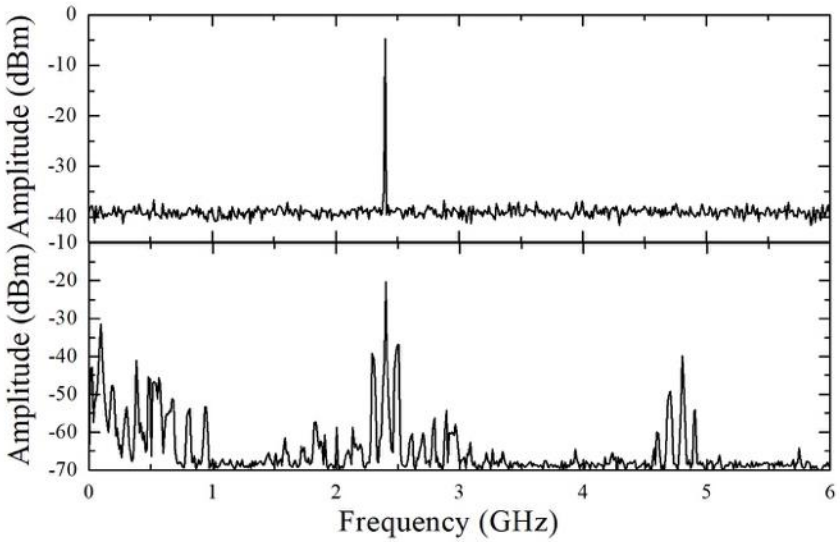

Figure 1-2. Effect of highly non-linear rectification stage in a 2.4 GHz signal. a) Full-Wave Rectifier b) Measured amplitude in dBm of the input signal. c) Measured Amplitude in dBm of the output rectified signal [11]

The final response of the bridge rectifier in Figure 1-3 (rectenna) shows a low-level spectral density in comparation with the received due to the non-linearity introduced by the diodes when these works at high frequency.

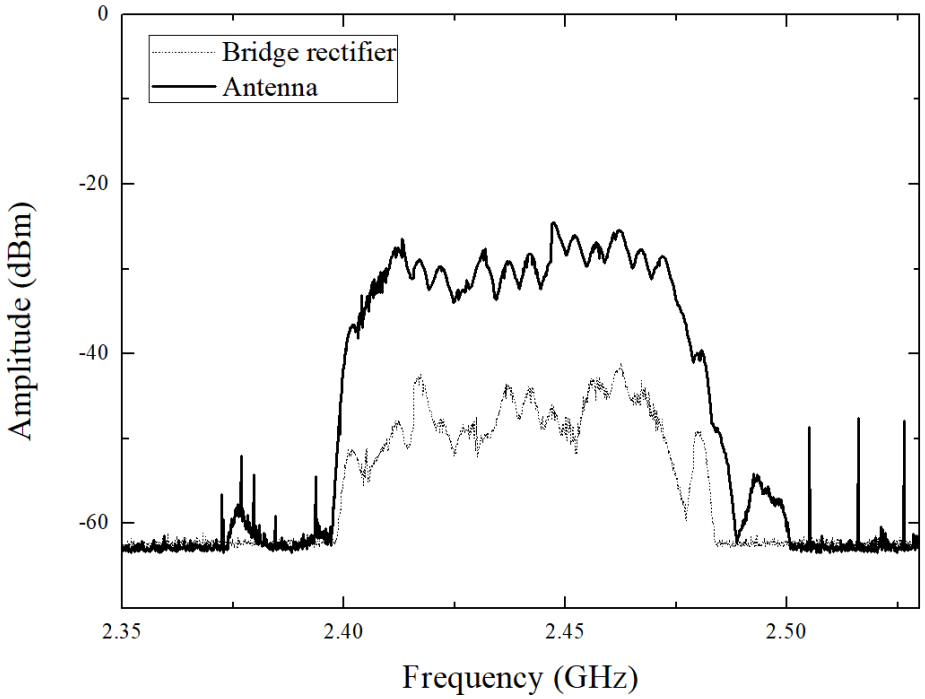

Figure 1-3. Spectral density by the antenna and rectenna [11]

To improve the power density captured by the rectenna, the RF transducer is confined by two metal layers (see Figure 1-4) producing multiple reflections of the near electromagnetic field, recreating the cavity Fabry-Perot [11]. Where the use of two surfaces very close together causes a multiple reflection out-of-phase of the RF signal from each other and that makes possible confine the RF power in the antenna enhancing the possibility to re-catch the reflected energy.

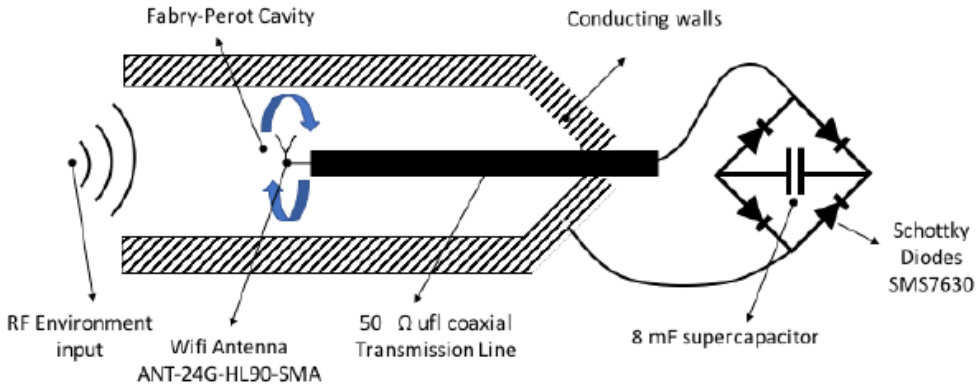

Figure 1-4. Scheme of RF-Energy Transducer: a standard antenna confined between the Fabry-Perot Cavity by metallic layers separated by a distance (GAP) around 0.1 mm. The output of the antenna is connected to a four Schottky diode rectifier bridge through a 50 UFL coaxial bridge [11]

In the chapter 3 is analysed the non-ideal environment and the power spectrum caught by the antenna (Figure 3-1) where it is detected that the energy is captured for more than a single frequency and therefore this will increase with the Fabry-Perot cavity.

The result of the enhanced RF transducer around of the 2.4 GHz band (Figure 1-5) shows an average improvement of 10 dBm.

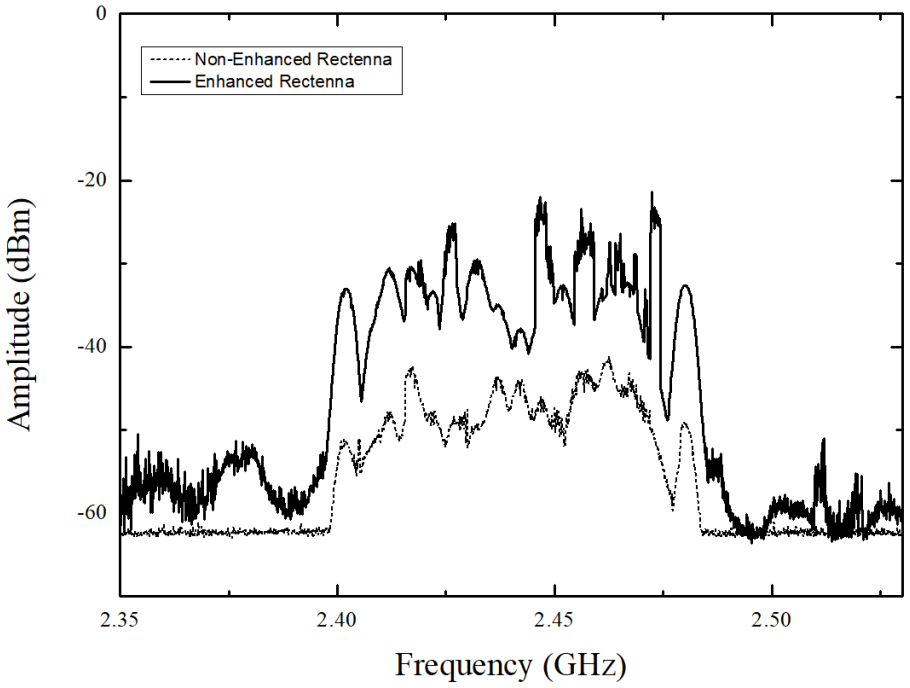

Figure 1-5. Spectrum power density of an enhanced rectenna and non-enhanced rectenna [11]

Each energy harvester system requires of a step-up stage based on an ultra-low power (ULP) due to the low energy and voltage generated and then be able to generate useful energy. This system applies a boost converter by the integrated circuit (IC) BQ25570 [12] from Texas Instrument composed by a DC power converter of high impedance able to pass the power in order of μW to mW. It also incorporates a buck converter DC-DC to adapt it to low consumption systems such as wireless sensor networks (WSN).

The improvement of the Fabry-Perot cavity (Figure 1-6) is increased 200 mV of average voltage and shows better results than rectenna.

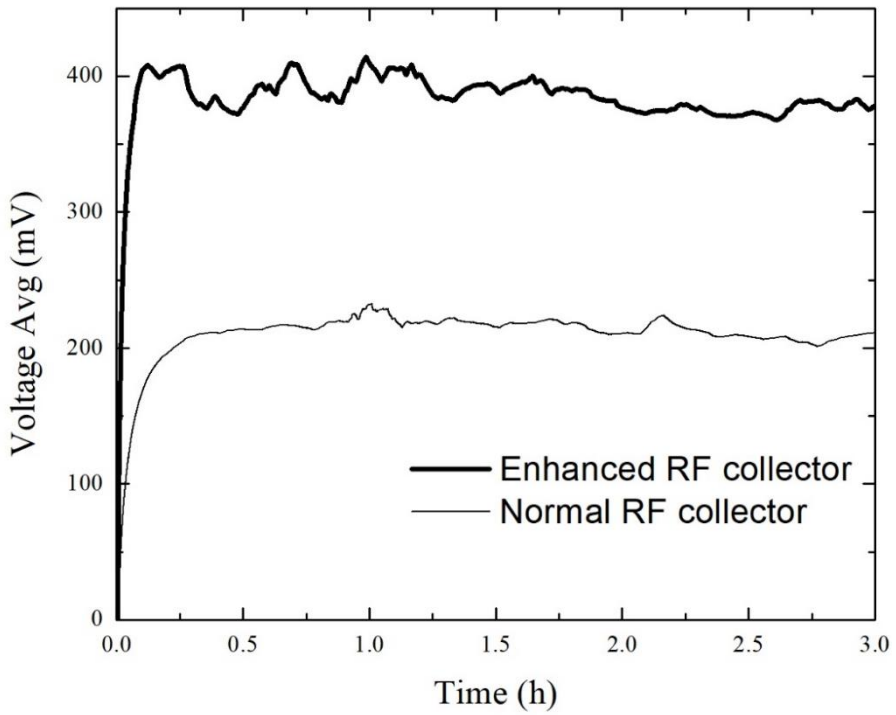

Figure 1-6. Performance comparison between the RF collector with a free antenna and with the Fabry-Perot cavity by a 4-wire set up using a N6705C DC Power Analyzer [13] with two N6781A modules [14]

The enhanced RF collector or transducer is viable as energy harvesting system taking account that minimal voltage required by the IC is 330 mV (see Annex 9.1). So, without the cavity the system would not work because it reaches a voltage lower than the required.

1.3 IEEE 802.11

The focus of the system is the capture of energy Wi-Fi waves for the 2.4 GHz band. IEEE 802.11 is standard part of the IEEE 802 [15] set of LAN protocols which allow the wireless connection between electronic devices under certain specifications. This standard defines the use of two lower levels of the physical layer and data link layer architecture, specifying the operating rules of a Wireless Local Area Network (WLAN). Within this standard there are different versions (Table 1-2) increasing in velocity, security or interworking between networks.

Standard	Year released	Band (GHz)	Bandwidth (MHz)	Maximum Data rate
802.11	1997	2.4	20	2 Mbps
802.11b	1999	2.4	20	11 Mbps
802.11a	1999	5	20	54 Mbps
802.11g	2003	2.4	20	54 Mbps
802.11n	2009	2.4/5	20/40	450 Mbps
802.11ac	2014	5	20/40/80/160	1.3 Gbps
802.11ax	2019	2.4/5	20/40/80/160	10 Gbps

Table 1-2. IEEE 802.11 standards development history in reference to frequency bands, bandwidth and maximum data rate

The first version was defined for three frequency ranges for the emissions at 2.4 GHz, 3.6 GHz and 5 GHz where was subdivided by channels with a 22 MHz of bandwidth. The spectrum at 2.4 GHz was divided into 14 channels with a separation of 5 MHz. Each country applies its own restrictions, for example in Europe are used 13 channels and North America only the first 11. On the other hand, the bandwidth of 22 MHz causes overlapping of adjacent channels, which can interfere with other devices working on other channels. The channels most used by the devices are usually 1, 6 and 11 (1, 5, 9 and 13 in some parts of the world).

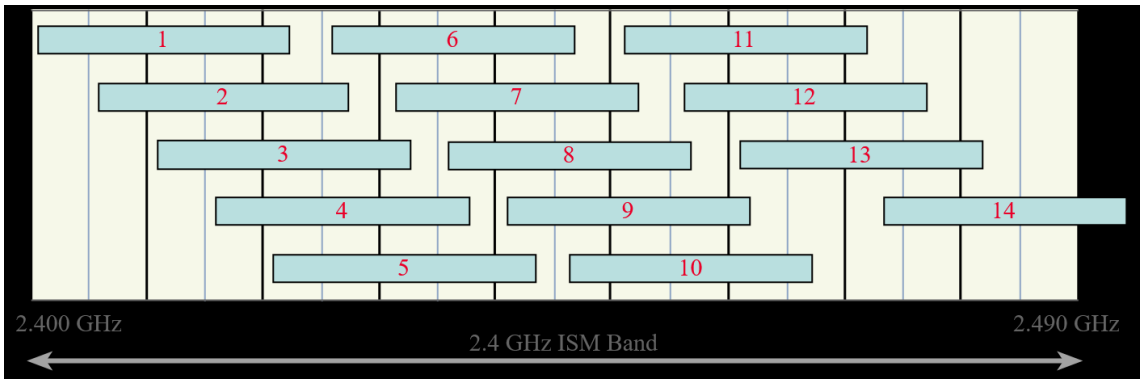

Table 1-3. Distribution of the channels into 2.4 GHz band [16]

In 802.11n version [17] there is the possibility of using signal bandwidths of either 20 MHz or 40 MHz. The difference is if the device uses the 40 MHz of bandwidth the number of channels used is reduce but increase the data throughput.

Then, for a working conditions analysis (chapter 3) we can determine the different Wi-Fi signals and specify the channels and bandwidth detected. On the other hand, the spectrum of the antenna is measure into 0-6 GHz frequency range (Figure 3-1) for the determination of the others works bands and see the energy collect in each one.

1.4 OBJECTIVES

The main objective of the present work is the parametric analysis of the proposed RF transducer performance in function of two metal layers, one up and one down, with different size and the separation distance (gap). This is realized for the analysis of confinement in RF antennas at Wi-Fi frequency bands by full 3D electromagnetic simulation on CST Studio [18] by the combination of the different solvers: frequential and integral equation.

RF antennas are designed and analysed to compare and discuss the behaviour to two commercial dipole antennas (Combo 47950-0001 [7] /47950-0011 [8]) by Molex which works on dual Wi-Fi band 2.4/5 GHz and a microstrip patch antenna at 2.4 GHz like a first academical approach and also like another alternative.

This report is based on previous experimental designs of the propose device such is the characterization in RF ambient radiated at Wi-Fi bands, power ranges or the quantity of charge accumulated.

In order to achieve the general objective, it have been necessary to realize the following technical tasks:

a. Definition of the work environment from a power spectral density for a commercial dipole antenna (Molex Combo 47950-0001) to extract the maximum available ambient power.
b. Design and definition of the result features such as the E-field or currents densities for a microstrip patch antenna at 2.4 GHz.
c. Design replicate of the commercial dipole antennas (Molex Combo 47950-0001 [7] / 47950-0011 [8]) at 2.4/5 GHz and definition of the result features.
d. Measurement of the maximum voltage achieve of the enhanced RF transducer for a measuring set-up with different size of metallic surfaces.
e. Behaviour and comparation of designed antennas from the E-field of the enhanced RF transducer with different metallic surface sizes at 2.4 GHz.

f. Efficiency and application of the enhanced RF transducer based on experimental measurement.

2 CST MICROWAVE STUDIO (CST MWS)

Microwave Studio (MWS) is an electromagnetic simulation software module of CST STUDIO SUITE [18] that allows full 3D electromagnetic analysis and design in the high frequency systems. For this reason, this software has been chosen and not another one.

The software provides several different simulation techniques:

a. **Transient solver:** Use a hexahedral grid in the mesh to obtain a good frequency response of the device from only one calculation run. It is used for high frequency applications like transmission lines, filters, antennas and others**.**
b. **Frequency domain solver:** For the structures electrically much smaller than the shortest wavelength, narrow bands problems (filters). Also contains fast methods calculation of S-parameters for strongly resonating structures.
c. **Integral equation solver:** Based on triangular surface mesh (very fine) for electrically large structures because volumetric discretization methods generally suffer from dispersion effects.
d. **Asymptotic solver:** Same that above but works for electrically extremely structures.
e. **Multilayer solver:** Is based on method of moments and does not require discretization of the transversally infinite dielectric and metal stack-up. Used for planar structures like microstrip filters in order to gain efficiency.
f. **Eigenmode solver:** Efficient method for calculate a finite number of modes in closed electromagnetic devices.

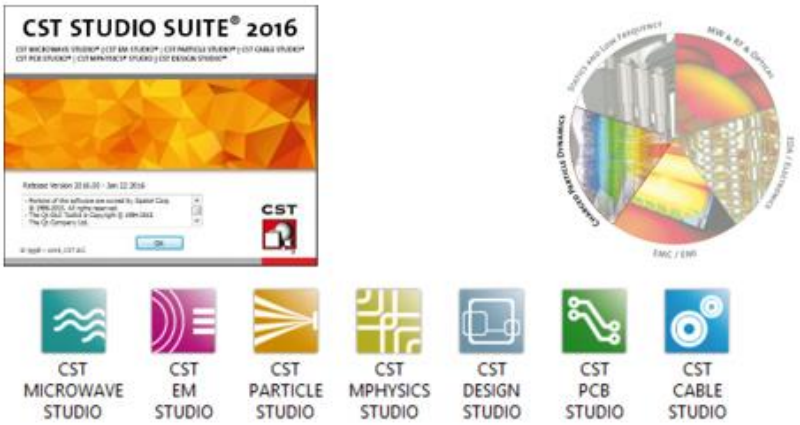

Figure 2-1. CST STUDIO SUITE modules

The combination of frequency domain and integral equation solver is applicated in this study.

A frequential mode can defines better and easily a good response of the reflection coefficient for the proposed antennas. However, not allow simulate the proposed RF transducer due to the application of the far-field source. So, the integral mode is tuned in an optimal mesh to difference accuracies to accomplish a similar reflection coefficient of the frequential domain to simulate the proposed RF transducer due to the application of the far-field source.

The simulation speed is around of 10/15 minutes by a considerable mesh and this time is increased up to 30 minutes to see for example the far-field, E-field or H-field.

3 WORKING CONDITIONS

Since the final objective of the work is to evaluate the viability of real harvesting systems, the measurement environment and de devices analysed have been chosen to be as close as possible to standard (non-controlled) environment and commercial antennas. The working conditions is considered like a non-ideal environment due to the distance of the Wi-Fi access point from the RF transducer (around of 4 meters), the attenuation of the walls of the laboratory, where the measurements will be carried out, and the radiation from the devices around it. The available RF environment energy can be estimated by measuring the frequential power density spectrum. To this end, the Rohde Schwarz FSL spectrum analyser in maximum power mode have been used [19].

Typical all-purpose Wi-Fi antennas have been chosen. For convenience due to their flatness, the Molex Combo antenna 47950-0001 operating at 2.4 GHz and 5 GHz [7], have been chosen. It is tested for the analysis of the environment and detect more power in 2.4 GHz than in 5.85 GHz, where the power spectral density is very poor (Figure 3-1). See for frequencies lower of 2 GHz a significant power detected where is located different services of communication (Table 3-1).

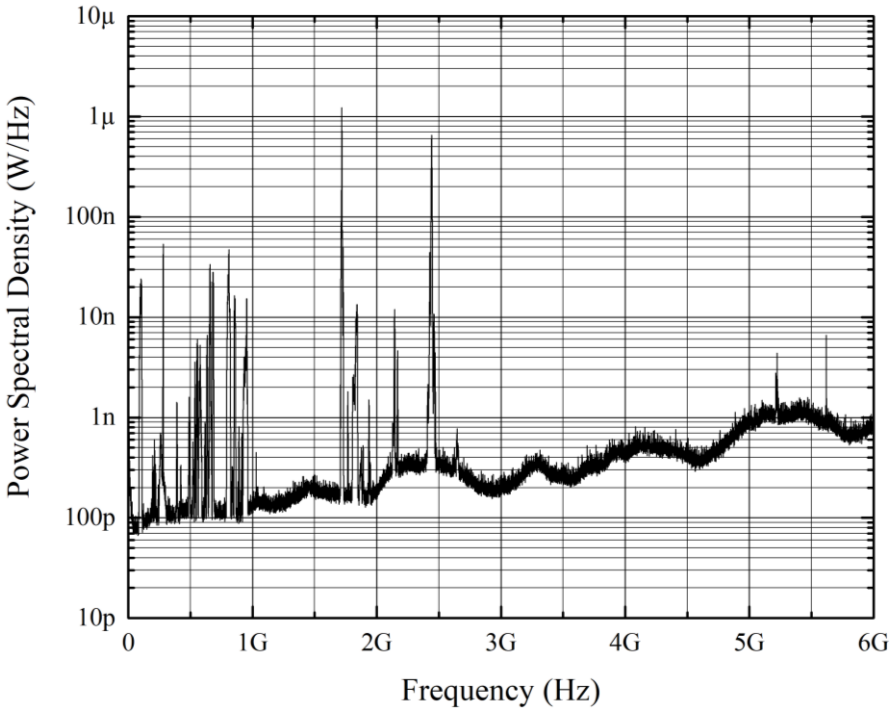

Figure 3-1. Power spectral density for the 47950-0001 Molex Combo antenna

In the Table 3-1 is showed the different services of communications and their frequency bands [20]:

Service		Frequency band
Mobile phone	4G/LTE	800/1500/1800/2600 MHz
	2G/GSM	900/1800 MHz
	3G/WCDMA	900/2100 MHz
GPS	GPS	1600 MHz
Radio broadcasting	FM	[87,5; 108,0] MHz
	AM (Europe)	[531; 1602] kHz
Digital Television	TDT	[470-800) MHz

Table 3-1. Different services of communications [20]

The above measure (Figure 3-1) corresponds with the power spectral density $S_{xx}(f)$with units of W/Hz, where the sum of all the integrals at each point is the result of the maximum available ambient power (Figure 3-2), obtaining at 1.8 GHz around of 15 μW, 25 μW for 2.4 GHz and 30 μW for 5 GHz.

$$P_{MAX} = \int_{-\infty}^{+\infty} S_{xx}(f)\, df \ \ [W] \tag{1.4-1}$$

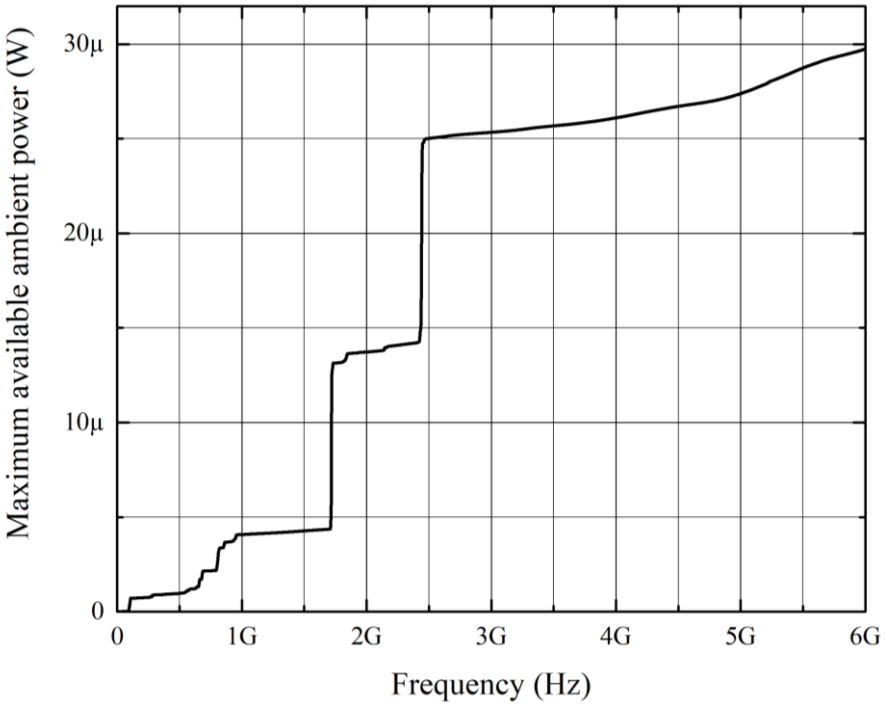

Figure 3-2. Maximum available ambient power for the 47950-0001 Molex Combo antenna

The graph showed in Figure 3-2 points out that, as expected, the more important contributions to the environment RF energy comes from the 1.8 GHz and 2.4 GHz. Just a few systems are actually radiating at 5GHz, being their contribution irrelevant to the overall amount of energy, even less important that the long-distance systems irradiating below 1 GHz (FM, AM base stations and GSM, for instance)

In Table 3-2 is showed the channels more used in the working conditions at 2.4 GHz by Wifi Analyzer application [21]. For the band of 2.4 GHz are the channels 1, 6 and 11. All networks works with 20 MHz of bandwidth except one with 40 MHz.

SSID	Band (MHz)	Channel	Signal (dBm)	Channel Width (MHz)
eduroam	2462	11	-87	20
CRAG	2462	11	-89	20
UAB	2462	11	-85	20
dEIC-research-2.4	2437	6	-94	40
UAB	2437	6	-95	20
UAB	2412	1	-74	20
eduroam	2412	1	-75	20
HUAWEI-B310-9091	2412	1	-89	20

Table 3-2. Channels into working conditions at 2.4 GHz

The resulting maximum available power in the environment depicted in Figure 3-2, obtained as a consequence of the calculation shown in equation (1.4-1), is the reference magnitude to evaluate the efficiency of the RF energy transducer.

4 RF ANTENNA

The RF system can be applied in various types of antennas such as a dipole, microstrip, Yagi, PIFA, monopole, etc. However, the selection comes down to microstrip and monopole antenna due to low cost, small size, planar and simple structure.

In this system design is chosen a two commercialized dipole antennas (Molex Combo antenna 47950-0001 [7] / 47950-0011[8]) which works on dual Wi-Fi band 2.4/5 GHz and a microstrip patch antenna at 2.4 GHz as an reference educational case and as another alternative to test on the simulated RF transducer in chapter 5.

For the purpose of compare the response of the different antennas, each antenna has been defined to see the features such as the E-field distribution or the reflection coefficient S_{11}.

4.1 MICROSTRIP PATCH ANTENNA

The theorical idea or first designs was introduce over 1950's by Deschamps [22] but it does not apply until 1970 [23],[24]. The microstrip breaks down in four types: printed slot, dipole, patch and travelling wave [25]. And some applications of these are for GPS systems, mobile phones, radars or biomedical systems.

The basic structure consists in a metal patch, which may be in a variety of shapes (the most common are the rectangular and circular), on top of a grounded dielectric substrate without losses and a ground plane (Figure 4-1). The dielectric substrate depends of the following design parameters:

- **Thickness:** typically, $0.003\lambda \leq h \leq 0.05\lambda$
- **Dielectric constant:** typically, $2.2 \leq \varepsilon_r \leq 12$

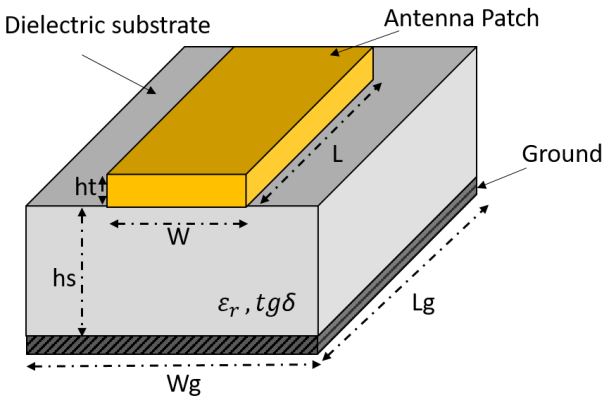

Figure 4-1. Microstrip antenna: metal patch on top of a grounded dielectric substrate

Dielectrics are characterized by the relative permittivity ε_r whose real part corresponds to the dielectric constant and the imaginary part with the losses. Which the both relations define the dielectric tangent loss (tg δ).

$$\varepsilon_r \triangleq \frac{\varepsilon}{\varepsilon_0} = \frac{\varepsilon'}{\varepsilon_0} - j\frac{\varepsilon''}{\varepsilon_0} = \varepsilon_r' - j\varepsilon_r' - j\varepsilon_r'' \qquad tg\delta \triangleq \frac{\varepsilon_r''}{\varepsilon_r'} \qquad (4.1\text{-}1)$$

Where, ε_r'' is the imaginary part and ε_r' the real part.

The dielectric constant and the tangent of losses are basic parameters in the design of microwave components based on dielectrics. They define: the propagation speed, the wavelength and the characteristic impedance in the case of the dielectric constant. Otherwise, it depends on the tangent of losses, the losses produced in the material. Any change in the properties of the materials can cause degradation of the material.

In the design of the patch antenna depends on the material dielectric substrate, will determine the wavelength which antenna can be exited and consequently the dimensions. A big dielectric constant will allow small dimensions, but it will be inefficient due to the losses it will have. Then, when this constant is lower the efficiency is high with large dimensions.

There are a different types of feeding techniques where the most common are the inset-fed, proximity coupling and the aperture coupling (Figure 4-2). These techniques present a high input impedance since the distribution of current is low at the ends of half-wave patch and increase toward the center. The distribution of the current allows through the positioning of the feed point, to adjust the input impedance, increasing it at the sides of the patch, where the current is minimum ($Z_{in}=V_{in}/I_{in}$) [26],[27].

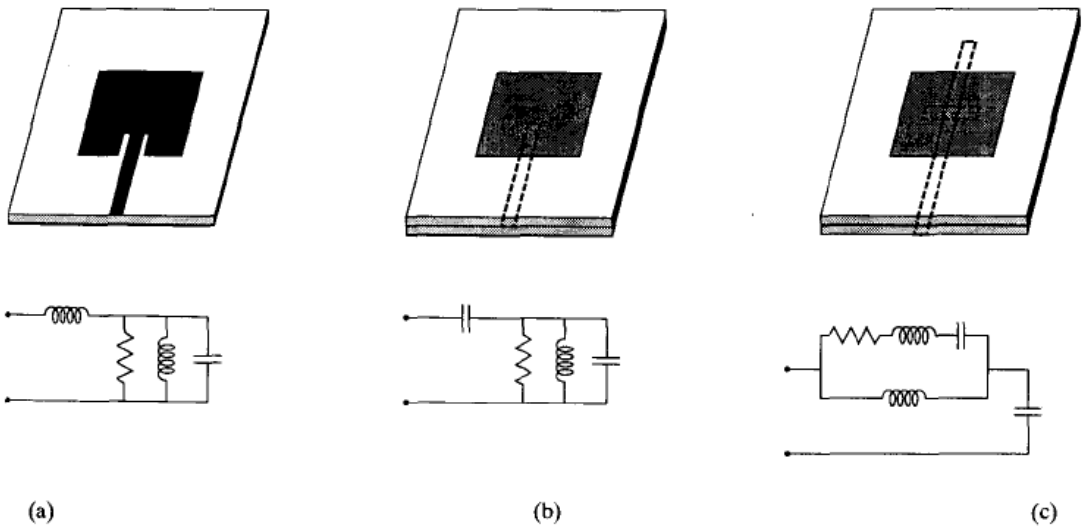

Figure 4-2. The different feeding methods with their equivalent circuits for microstrip antennas. a) Inset-fed. b) Patch proximity coupled to a microstrip feed line. c) Patch aperture coupled to a microstrip feed line [27]

Each method of feeding has advantages and disadvantages in the design and response but not are taking account for the application at the RF transducer. So, for the study of the antenna is apply a simple design with the inset-fed method.

4.2 PATCH ANTENNA DESIGN AND SIMULATION

Is designed and defined the features for the patch antenna such as the design parameters, return losses (S_{11}), radiation pattern, gain and impedance with the CST Studio simulation tool in order to apply and compare with others antennas in the enhanced RF transducer (chapter 5).

4.2.1 Design of a patch antenna

In this section is calculated the dimensions to create a patch antenna to work at 2.4 GHz with a dielectric substrate Roger RO3010 with 1.27 mm thickness, tangent losses of 0.002 and dielectric constant ε_r=10.2. The material used is a perfect electric conductor (PEC) for the ground and patch to avoid added losses.

Chosen an inset-fed technique, the dimension of antenna consists of the parameters showed in the following figure:

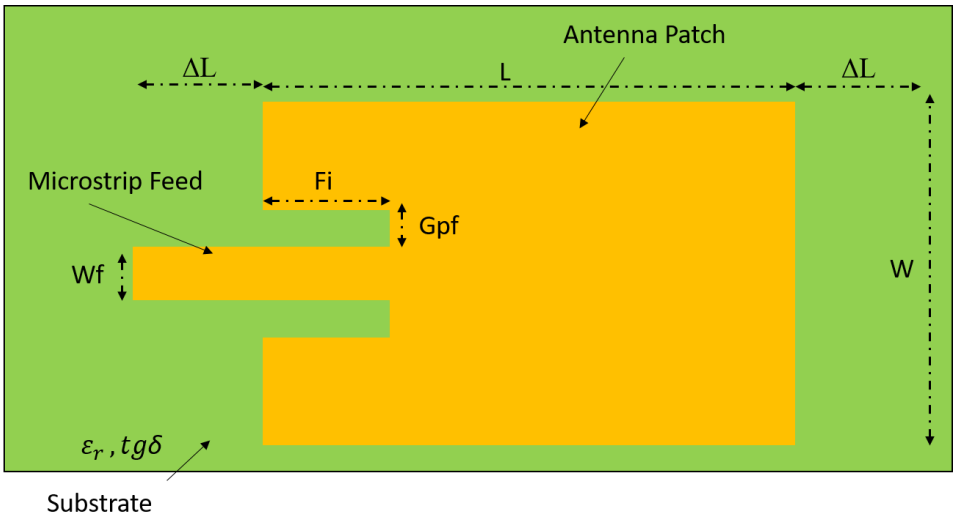

Figure 4-3. Top view of rectangular microstrip feed line (inset-fed)

Which the gap between the patch and the inset-fed (*Gpf*) is normally 1 mm.

Firstly, is find the transmission line width W:

$$W = \frac{c}{2f_c}\sqrt{\frac{2}{\varepsilon_r + 1}} = \frac{3 \cdot 10^8}{2 \cdot 2.4 \cdot 10^9} \cdot \sqrt{\frac{2}{10.2 + 1}} = 26.41\ mm \tag{4.2-1}$$

And then, the other parameters are calculated as well as the effective dielectric constant:

$$\varepsilon_{reff} = \frac{\varepsilon_r + 1}{2} + \frac{\varepsilon_r - 1}{2}\left(1 + 12\frac{h}{W}\right)^{-0.5} \xrightarrow[\substack{\varepsilon_r=10.2 \\ W=26.4\ mm}]{h=1.27\ mm} \varepsilon_{reff} = 9.26 \tag{4.2-2}$$

The next step is to calculate the effective length given as:

$$L_{eff} = \frac{\lambda}{2\sqrt{\varepsilon_r}} = \frac{c}{2f_c\sqrt{\varepsilon_r}} = \frac{3 \cdot 10^8}{2 \cdot 2.4 \cdot 10^9 \cdot \sqrt{10.2}} = 20.5\ mm \tag{4.2-3}$$

The extended length (ΔL) is determined due to the fringing field caused by the width and position of feed antenna. It is an effect that produces an increase of the radiation obtaining a directive radiation and consequently a shift in the operation frequency.

$$\Delta L = 0.412h\frac{\left(\varepsilon_{reff} + 0.3\right)\left(\frac{W}{h} + 0.264\right)}{\left(\varepsilon_{reff} - 0.258\right)\left(\frac{W}{h} - 0.8\right)} \xrightarrow[\substack{\varepsilon_{reff}=9.26 \\ W=26.4\ mm}]{h=1.27\ mm} \tag{4.2-4}$$

$$\Delta L = 0.585\ mm$$

So, the real length of the patch is:

$$L = L_{eff} - 2\Delta L = 19.36 - 2 \cdot 0.585 = 19.36\ mm \tag{4.2-5}$$

To calculate the feed line width *Wf*, is used the *Impedance Calculation* tool of CST defining the frequency, thickness of substrate and the dielectric constant (see Figure 4-4). Obtaining a feed line width of 1.2 mm and the input impedance equal to 50 Ω.

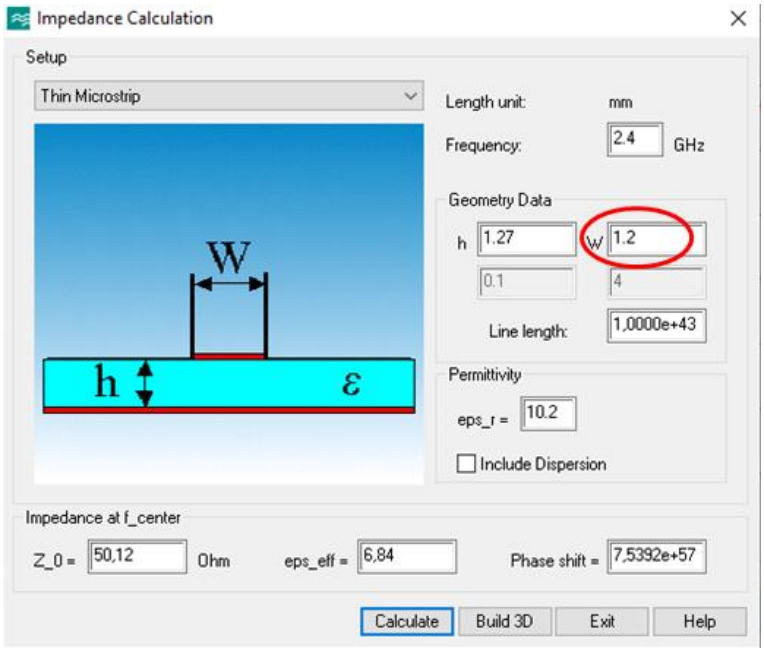

Figure 4-4. Impedance Calculation tool into CST

With the above parameters, input impedance and width of microstrip feed line, can be calculated the length of inset named as *Fi*.

$$Fi = 10^{-4}(0.001699\varepsilon_r^7 + 0.13761\varepsilon_r^6 - 6.1783\varepsilon_r^5 + 93.187\varepsilon_r^4 - 682.69\varepsilon_r^3 + 2561.9\varepsilon_r^2 - 4043\varepsilon_r + 6697) \cdot \frac{L}{2} \tag{4.2-6}$$

For a *L*=19.36 mm and a dielectric constant of 10.2 mm the result in (4.2-6) equation is 8.29 mm.

And the ground dimensions are defined by:

$$W_g = 2W \qquad L_g = 2L \tag{4.2-7}$$

In short, the antenna design parameters are:

Parameters	Value [mm]	Description
W	26.4	Width of transmission line
L	19.36	Length of transmission line
Fi	8.29	Length of inset
Wf	1.2	Width of microstrip feed line
Gpf	1	Gap between the patch and the inset-fed
Lg	38.73	Length of ground
Wg	52.82	Width of ground
hs	1.27	Substrate thickness
ht	0.035	Conductor thickness

Table 4-1. Parameters design of the microstrip antenna

4.2.2 Simulation of the patch antenna

From the parameters of the Table 4-1, a dielectric substrate of Rogers RO3010, a perfect electric conductor (PEC) for the ground and patch to avoid added losses and a port feeding of 1 V and 50 Ω is define the main features of the antenna.

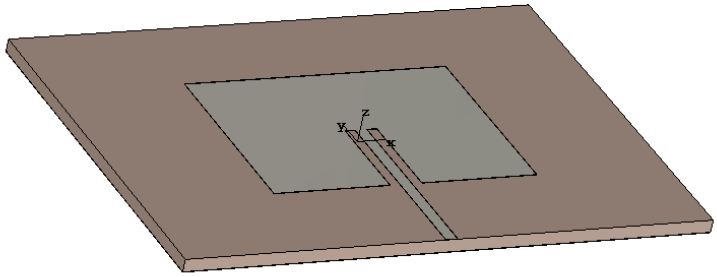

Figure 4-5. Model of the inset-fed patch antenna for a finite substrate (Rogers RO3010)

The coefficient response with maximum adaptation (Figure 4-6) for a *L* designed corresponds with a frequency of around 2.36 GHz to -18.9 dB and bandwidth at -10 dB of 9.2 MHz. The response is slightly smaller than the operation frequency calculated. This fact may be due to the variation sensibility in the antenna length and an error in the converged solution.

To correct the length variation, this factor have to decrease to adjust at 2.4 GHz because this parameter control the modes frequency denotated by *n* to the cavity model Figure

4-7. Then, if *L* is multiplied by a factor *a*, where is defined like a central frequency result over the require, is obtained a frequency more accurate than the designed.

$$a = \frac{f_0\ (result)}{f_0\ (required)} = \frac{2.36\ GHz}{2.4\ GHz} = 0.983 \tag{4.2-8}$$

$$L_{adjusted} = L_{designed} \cdot a = 19.36 \cdot 10^{-3} \cdot 0.983 = 19.07\ mm$$

At the same time, it can show the reflection coefficient and bandwidth decrease when the length of the patch is changed. These effect not is important for the present work, but this change can be defined by the losses of the material in *Fi* parameter.

A characteristic of the inset-fed patch antenna is the narrow bandwidth as is showed in the reflection coefficient (Figure 4-6) and the following calculation of the FBW (fractional bandwidth) in (4.2-9) at the adjusted length. It is a low value.

$$FBW = \frac{BW}{f_0} \cdot 100 = \frac{0.008\ GHz}{2.4\ GHz} \cdot 100 = 0.33\% \tag{4.2-9}$$

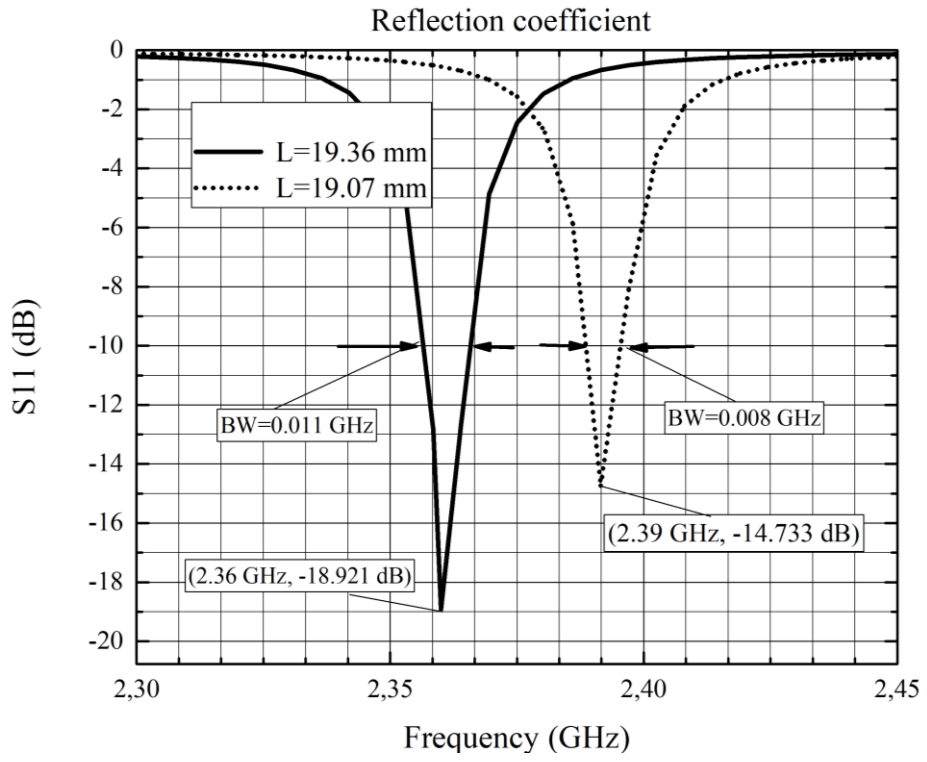

Figure 4-6. Reflection coefficient of the inset-fed patch antenna for a L parameter designed and L adjusted

For a sweep at range of 1 GHz to 6.5 GHz, is identified the operation modes of a patch antenna, see Figure 4-7, following the cavity model described in (4.2-10).

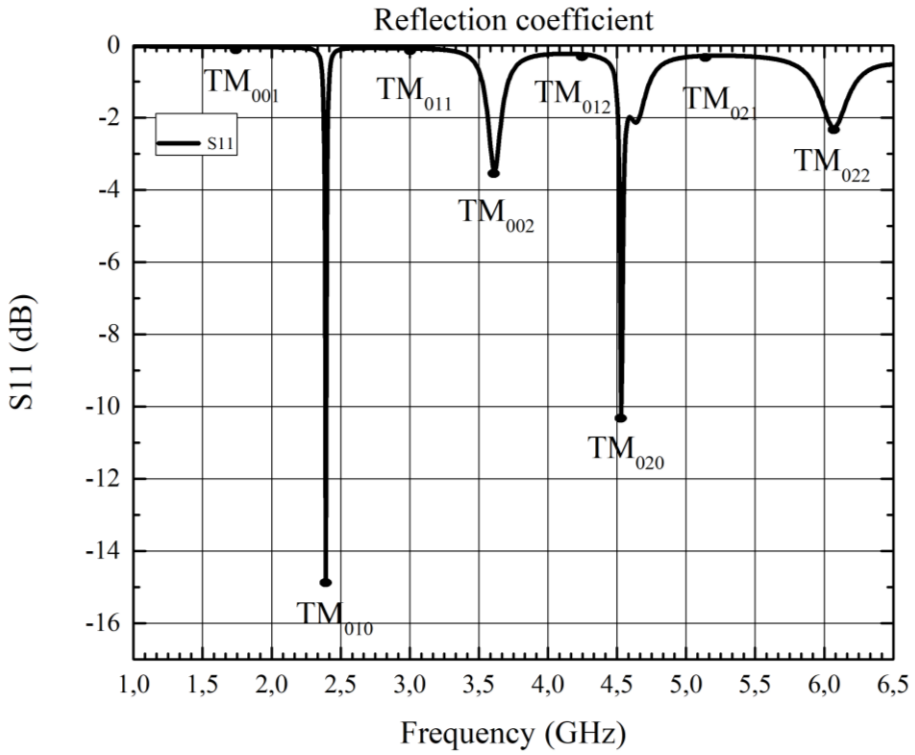

Figure 4-7. Propagation modes of the inset-fed patch antenna

Modes propagation changes respect to the feeding point position:

$$(f_r)_{mnp} = \frac{1}{2\pi\sqrt{\mu\varepsilon}}\sqrt{\left(\frac{m\pi}{h}\right)^2 + \left(\frac{n\pi}{L}\right)^2 + \left(\frac{p\pi}{W}\right)^2} \tag{4.2-10}$$

Where,

$$m = 0, 1, 2 \ldots \quad n = 0, 1, 2 \ldots \quad p = 0, 1, 2 \ldots$$

$$m = n = p \neq 0 \ (simultaneously)$$

TM mode	**001**	**010**	**011**	**002**	**012**	**020**	**021**	**022**
f_r (GHz)	1.78	2.43	3.01	3.56	4.31	4.85	5.17	6.02

Table 4-2. TM modes of the inset-fed patch antenna

Depends of the distribution of cavity field, the modes can be exited or not. If the alimentation is located for a null field and it is not accorded with the feeding, the final adaptation will be bad. Otherwise, when the feed and the cavity field concorded, will have a good adaptation. Note in the previous Figure 4-7 that first mode is TM_{010} due to the feed is according to the alimentation of this mode, but when the feed is in W/2 to L*0.3, Figure 4-8, the response change to TM_{0X2} modes.

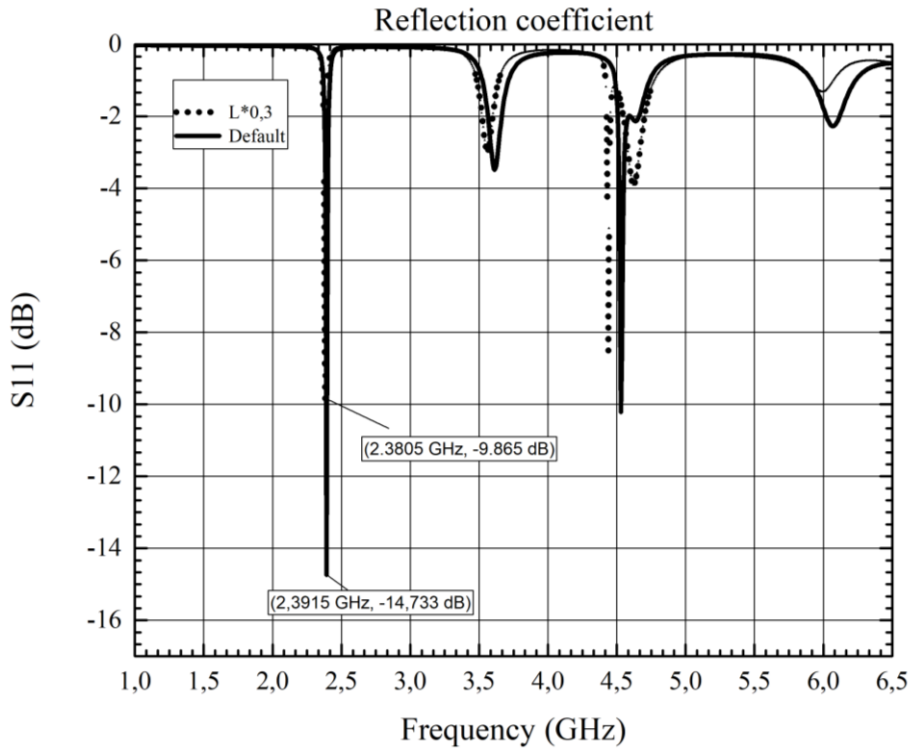

*Figure 4-8. Reflection coefficient for a feeding point in W/2 and two different L positions: L default and L*0.3*

For others like TM_{0X1}, the feeding point must have different that W/2, along the X-axis, where the field of the modes is null. And the mode defines for *m* (i.e. TM_{100}, TM_{110}...) are determined by the height *h* (along Z-axis).

The impedance for L=19.07 mm (Figure 4-9) at 2.3915 GHz is 38.18-j9.64 Ω while at 2.3969 GHz it is around 50 Ω, so it means a good adaptation. Both impedances have a capacitive behaviour.

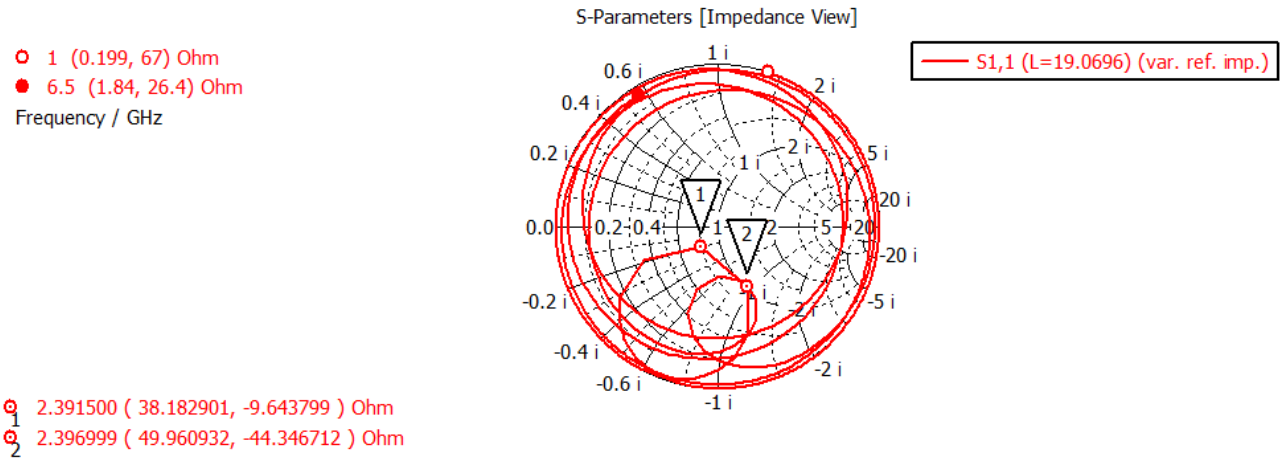

Figure 4-9. Smith chart of the inset-fed patch antenna for L=19.07 mm

At the resonant frequency, the more intense current density is located at the center of the antenna and it decreases at the ends (Figure 4-10). It is characteristic of a half-wave patch and the input impedance could be reduced if the patch was fed closer to the center by the design parameter *Fi* [26].

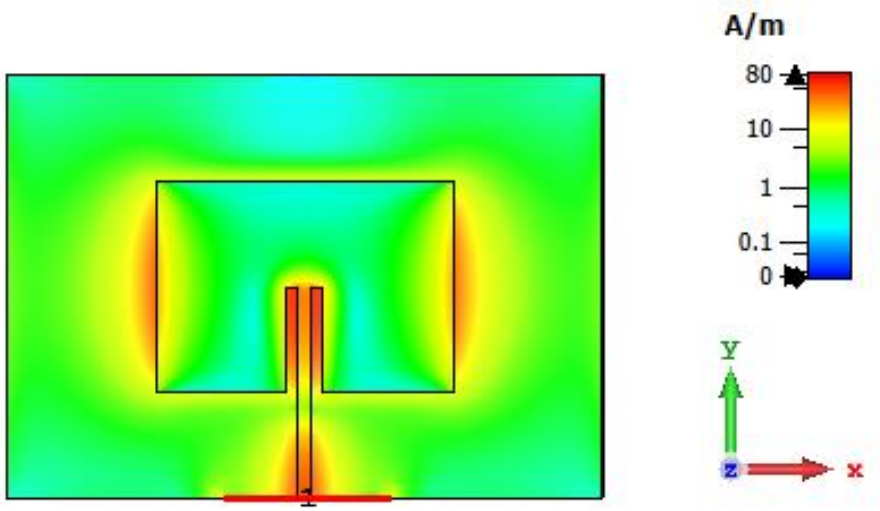

Figure 4-10. Current density of the inset-fed patch antenna at 2.4 GHz

In Figure 4-11 is showed the typical directive behaviour of radiation pattern with a maximum gain of 5.9 dBi at 2.4 GHz. Also, it can be observed the loss of energy in the above of the antenna due to the infinite plane defined like a perfect electric conductor (PEC).

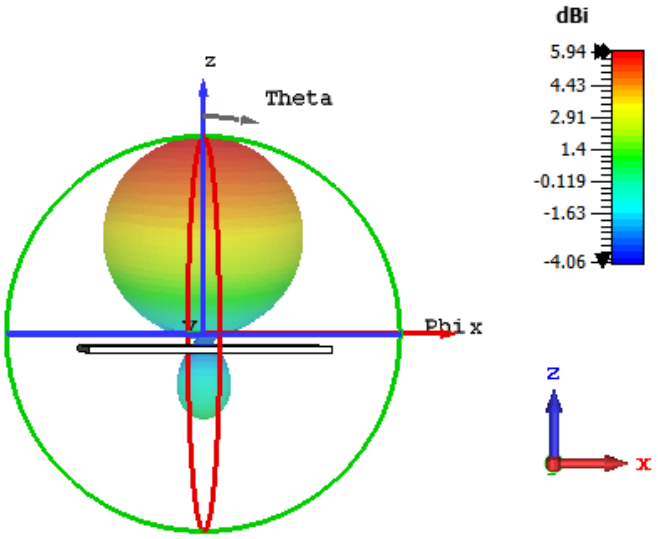

Figure 4-11. Radiation pattern at 2.4 GHz in inset-fed patch antenna

Finally, the electric distribution of the inset-fed patch antenna is illustrated at 2.4 GHz (Figure 4-12).

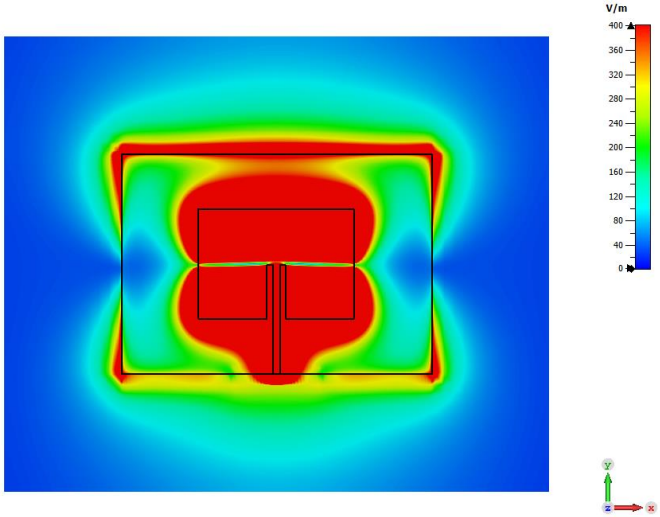

Figure 4-12. E-field distribution of the inset-fed antenna at 2.4 GHz

It is maximum at sides along the Y-axis and zero from the center of the antenna along the X-axis.

The features results obtained are used to see the behaviour of the antenna such as the frequency of resonance, the geometry or electric field distribution in order to compare some differences in the application of the resonant cavity (chapter 5).

4.3 DIPOLE ANTENNAS

A dipole antenna is defined by two conductors fed into the center, where the half-wave dipole is the type more commonly used (see Figure 4-13) and characteristic due to the total length is proportional to half wavelength of the resonant frequency giving rise to a low impedance of 73 Ω. The low impedance allow matching to the line to be nearly at characteristic impedance of 50 Ω and 75 Ω.

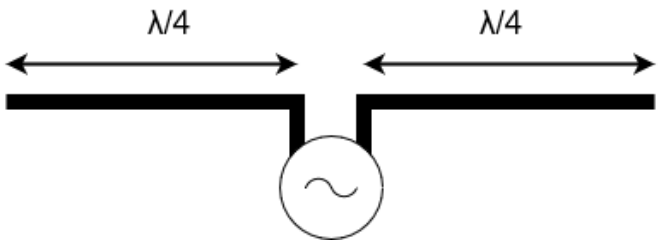

Figure 4-13. Half-wave dipole antenna

In this case, the distribution of the current has a sinusoidal form with the minimums at the ends and the maximum at the feeding point. In contrast, the voltage which is also vary sinusoidally is low at the middle and rises to the top at the ends.

Other case of finite length dipole is called small dipole because the total length is lower than the half wavelength. It contains a large capacitive reactance and requires an inductance load at the end of the antenna or other matching network. The distribution of current is triangular.

Furthermore, exist other variants of the dipole such as the folded dipole antenna, this is a half wave dipole with a two connections parallel wire at the ends. And also, the multiple half waves dipole antenna which use of an odd multiple of half wavelengths long [26].

4.4 DIPOLE ANTENNAS STRUCTURE DESCRIPTION, EXPERIMENTAL MEASUREMENTS AND SIMULATION

The following point describes the dipole antennas for the design in CST Studio simulation tool, is realized experimental measurements to obtain the reflection coefficient S_{11} and approach the simulation response with an optimal mesh. Also, in the simulation is describes the features such as the radiation pattern, gain and impedance in order to apply and compare with others antennas in the enhanced RF transducer (chapter 5).

4.4.1 Structure description of the dipole antennas

Two models of dipole antenna are used. Both are dual band operating at 2.4 GHz and 5 GHz for a different geometries (Figure 4-14 and Figure 4-16) but similar behaviour (Table 4-3). In the first case, the Molex Combo antenna 479500001 [7] is narrower with a complex design in comparation the other model showed in Figure 4-16.

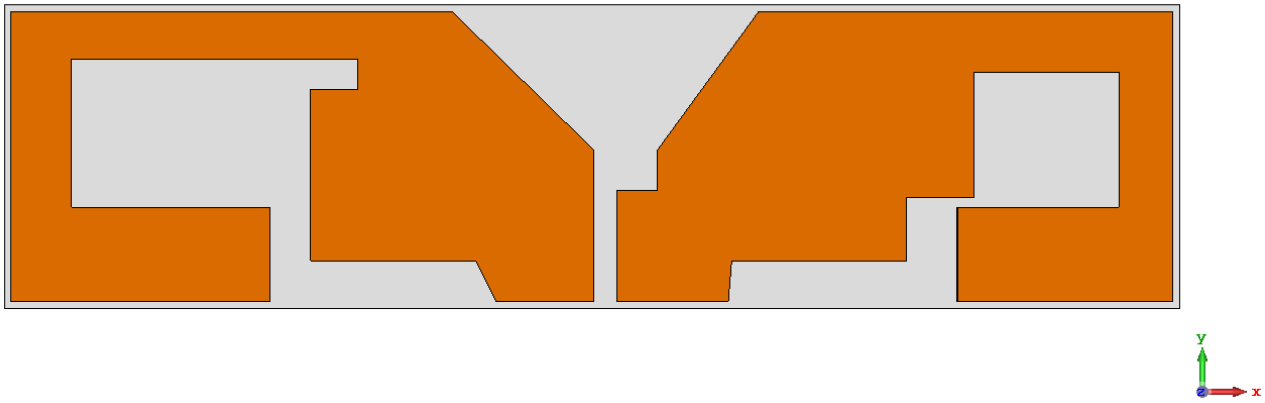

Figure 4-14. Layout of Molex Combo antenna 47950-0001, where the orange area corresponds with the dielectric layer and the grey area with the substrate

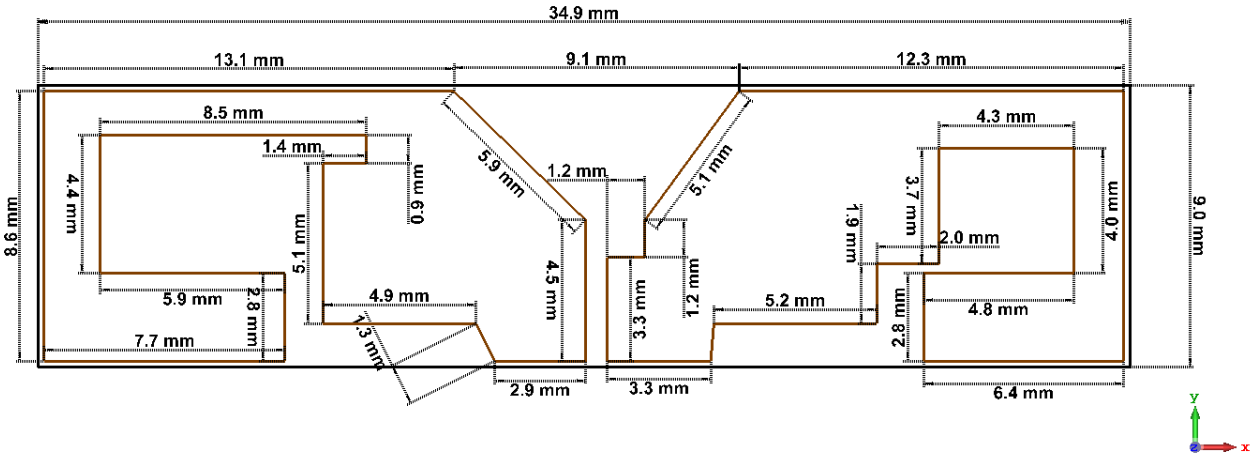

Figure 4-15. Dimensions of the geometry of the Molex Combo antenna 47950-0001, where the orange area corresponds with the dielectric layer and the grey area with the substrate layer

For the second case, the Molex Combo antenna 47950-0011 it shows a design easier and the similar central structure is maintained in reference of the invers triangle. Also, the gap between the substrate and the dipole is the same of 0.2 mm.

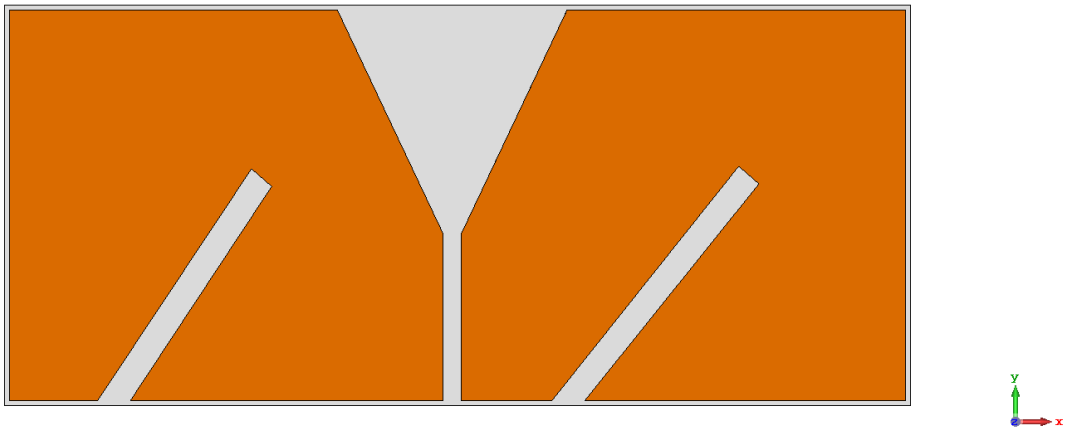

Figure 4-16. Layout of Molex Combo antenna 47950-0011, where the orange area corresponds with the dielectric layer and the grey area with the substrate layer

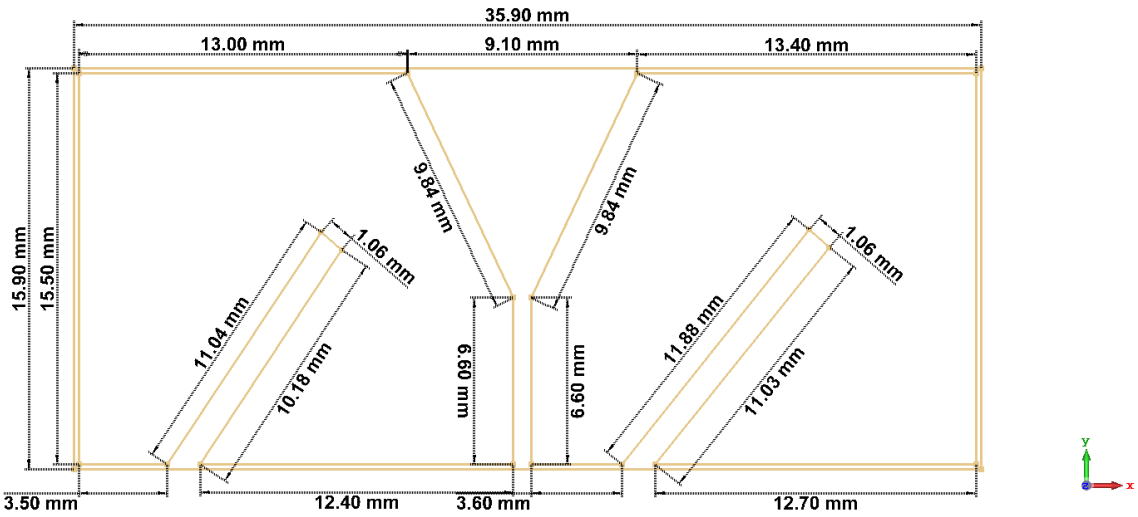

Figure 4-17. Dimensions of the geometry of the Molex Combo antenna 47950-0011, where the orange area corresponds with the dielectric layer and the grey area with the substrate layer

Both antennas are manufactured in a 50 µm flexible substrate material called polyimide (PI) with a dielectric constant 3.5 and a loss tangent of 0.002. The characteristic of this flexible substrate for the antennas manufactured is the low-cost materials, flexibility and strength. Concretely the polyimide (PI) is the most used to the industry for the low loss factor over a wide frequency range for a loss tangent of 0.002 and a dielectric constant of 3.2 to 3.5.

The copper layer is 20 µm thickness. Besides of these layers, exist an adhesive layer which increase the total thickness (described in the datasheets) of the antenna producing possible losses [7],[8]. It should be taken into account for the reflection coefficient study.

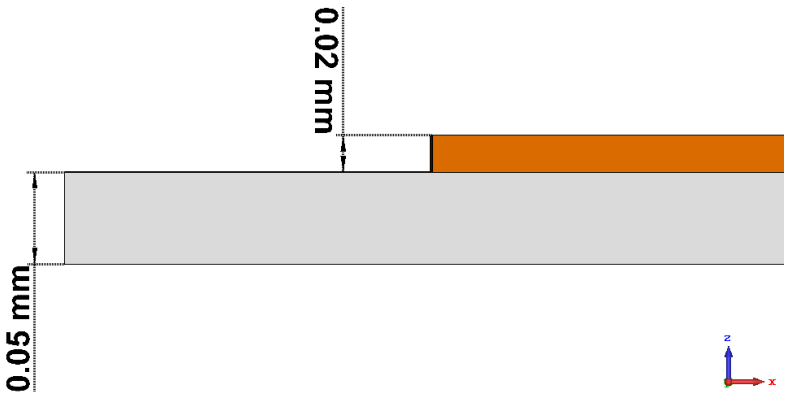

Figure 4-18. Layers of the Molex Combo antennas. Polyimide substrate (grey) and copper metal layer (orange) separate by a gap of 0.2 mm.

The dimensions in Figure 4-15 and Figure 4-17 have been obtained with Microscope Leica M80 [28] where is necessary a configuration by each augment in the microscope (Figure 4-19.a).

a)

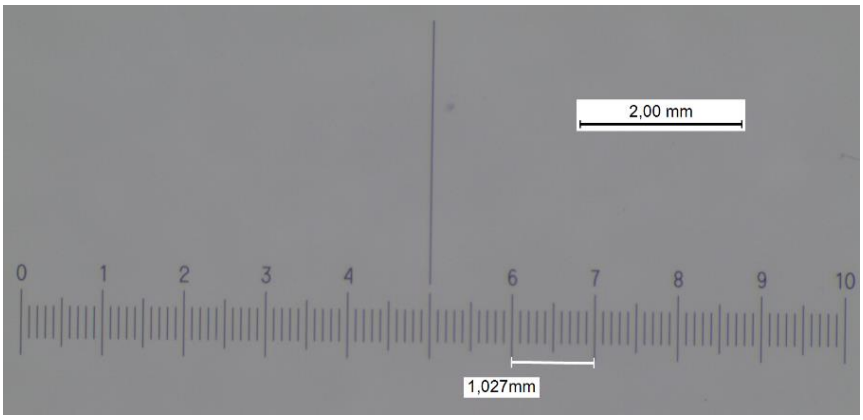

b)

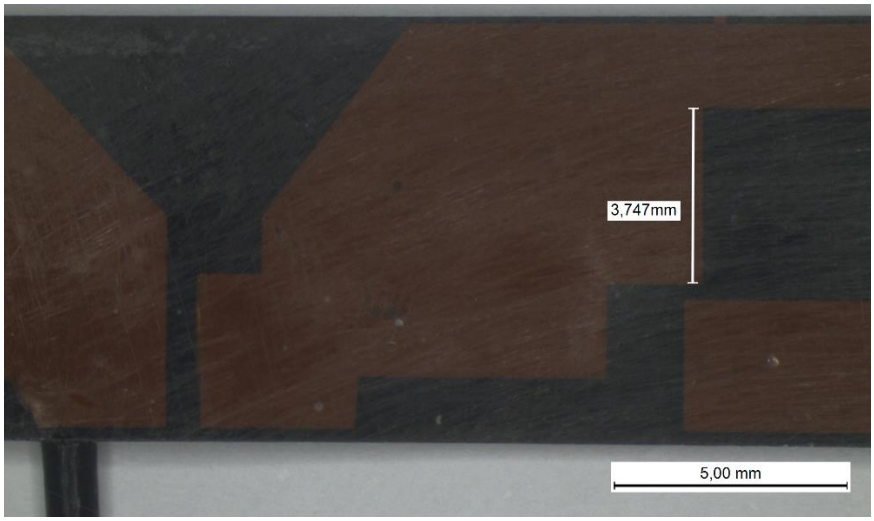

Figure 4-19. Measurement set-up using a Microscope Leica M80 [28]. a) Configuration calibration for x1.25 augment. b) Example of the measurement of the Molex Combo antenna 479500001 for x0.75 augment

In the following Table 4-3, are described the electrical specifications of the models where the newest model 47950-0011 (second case) is more efficient at 2.4/5 GHz and the peak gain is increased around 6 % at 5 GHz but as a consequence the gain at 2.4 GHz is worse, decrease around of 24 %. The gain is the most important characteristic of an antenna because is the relationship between the field intensity produced by an antenna at a given point, and the field intensity produced by an omnidirectional antenna knows as isotropic, at the same point and under the same conditions.

Instead the two resonant frequency and the return loss (S_{11}) are maintained values.

Antenna 47950-XXXX	**Range Band #1 (MHz)**	**Range Band #2 (MHz)**	**Electrical Connectivity**	**Peak Gain (dBi)**	**S11 (dB)**	**Total Efficiency**
-0001	(2400 - 2483.5)	(4800-5900)	Cable	3.0 @ 2.4 GHz 4.6 @ 5 GHz	<-10 <-9	>75% @ 2.4 GHz >70% @ 5 GHz
-0011	(2400 - 2483.5)	(4800-5900)	Cable	2.27 @ 2.4 GHz 4.9 @ 5 GHz	<-10 <-9	>85% @ 2.4 GHz >85% @ 5 GHz

Table 4-3. Electrical specifications of the two models Molex Combo antennas [7], [8]

In summary, the parameters of the design in CST Studio are defined in Table 4-4:

Parameters	Value [mm]		Description
	Antenna 47950-0001	**Antenna 47950-0011**	
W	34.9	35.9	Width of transmission line
L	9	15.9	Length of transmission line
hs	1.27	1.27	Substrate thickness
hd	0.035	0.035	Metal thickness
g	0.2	0.2	Gap between the substrate and metal structure

Table 4-4. Parameters design of the Molex Combo antennas

Where is based on the measures in Figure 4-15 and Figure 4-17.

4.4.2 Experimental measurements and simulation of the dipole antennas

Measurement of the reflection coefficient in a test range of 9 KHz to 6 GHz with a differential port feeding port of 1 V and 50 Ω with the VNA E8357A [29]. The measure will be used to find the best mesh to obtain a similar simulation response. Before, the VNA it should be calibrated by a kit 85521A [30] and with the adapters to connect the dipole antenna.

a)

b)

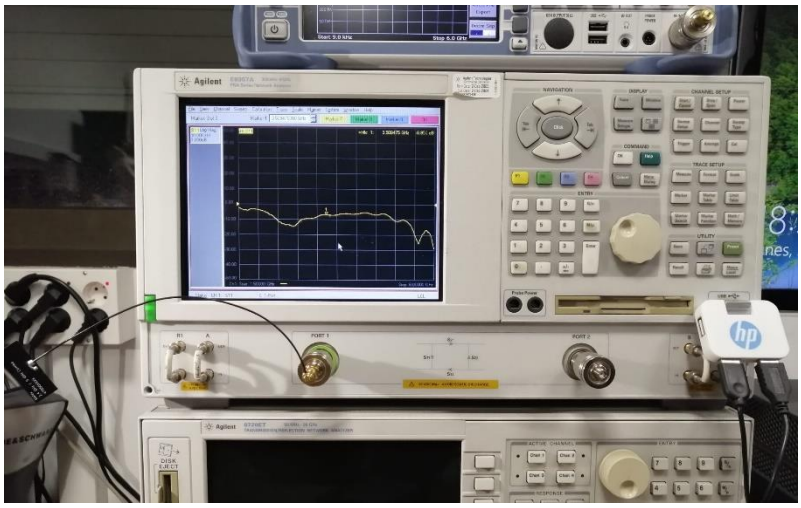

Figure 4-20. Measure of the dipole antenna with the VNA. a) View of the adapters and connexions of the dipole antenna. b) Example about the S_{11} parameter measured

The reflection coefficient for the antenna 47950-0001 is then simulated to be compared with the measurement (Figure 4-21), which shows a similar response and a possible approximation with a dielectric constant of 3.

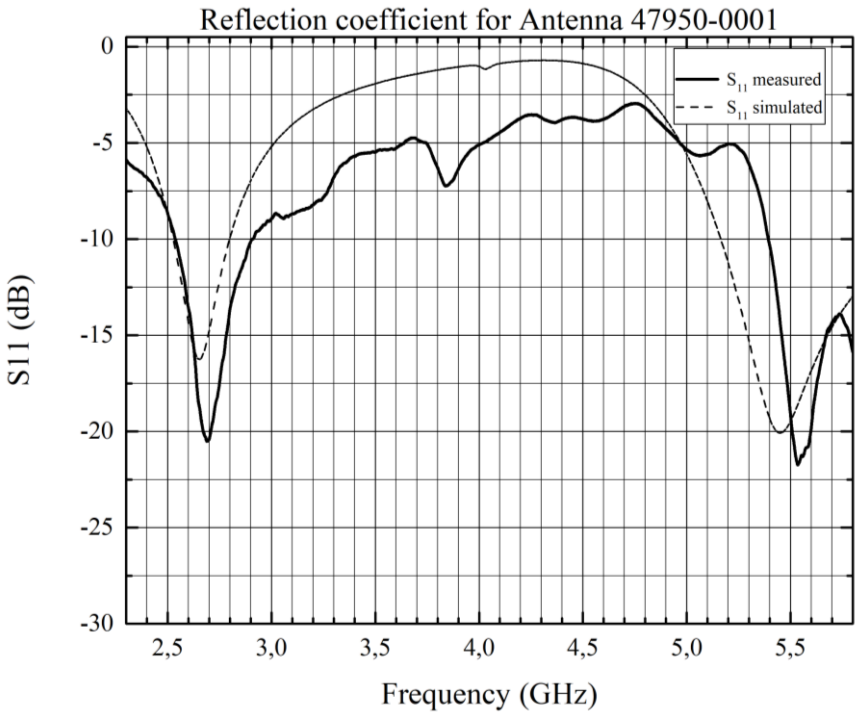

Figure 4-21. Reflection coefficient for the antenna 47950-0001

If the constant ε changes, the response is moved to high frequencies when it decreased and a opposite response when it is increased due to design parameters. In Figure 4-22, the dielectric constant is changed to 3 and 4 maintaining the above value in 3.5, being able to observe changes are noticeable for the second resonant frequency in comparation of the

first resonance. So, for a dielectric constant of 3 the response is adjusted in frequency for other values, but the adaptation peak is worsted and in spite of this, is maintained ε=3.5 to continue the study.

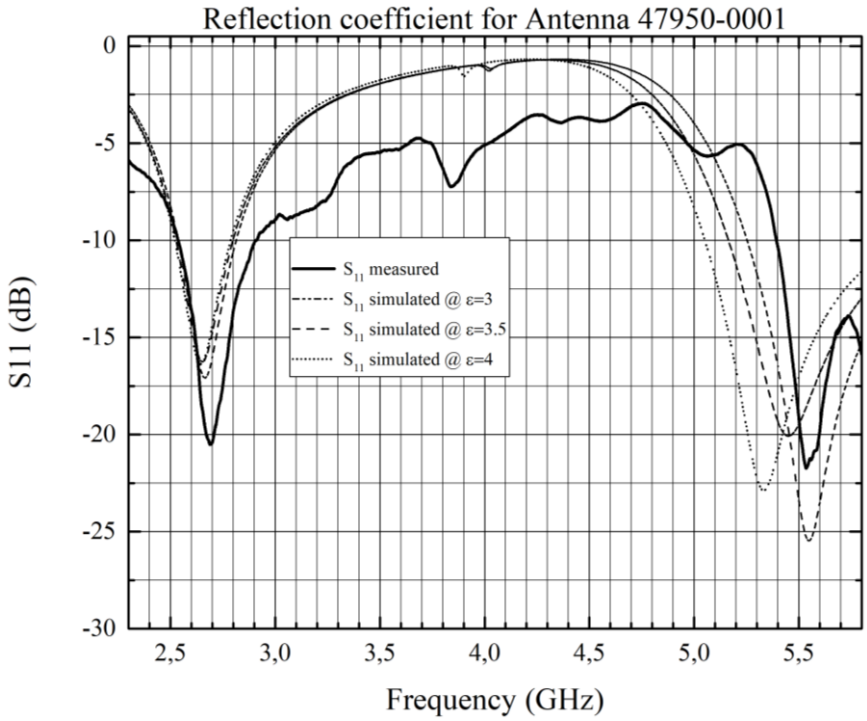

Figure 4-22. Reflection coefficient for the antenna 47950-0001 at 3, 3.5 and 4 to the dielectric constant

In Figure 4-23 the simulation mesh has been changed to improve the calculation accuracy of the response, so it has become more like the real measure. The first resonance frequency is more similar.

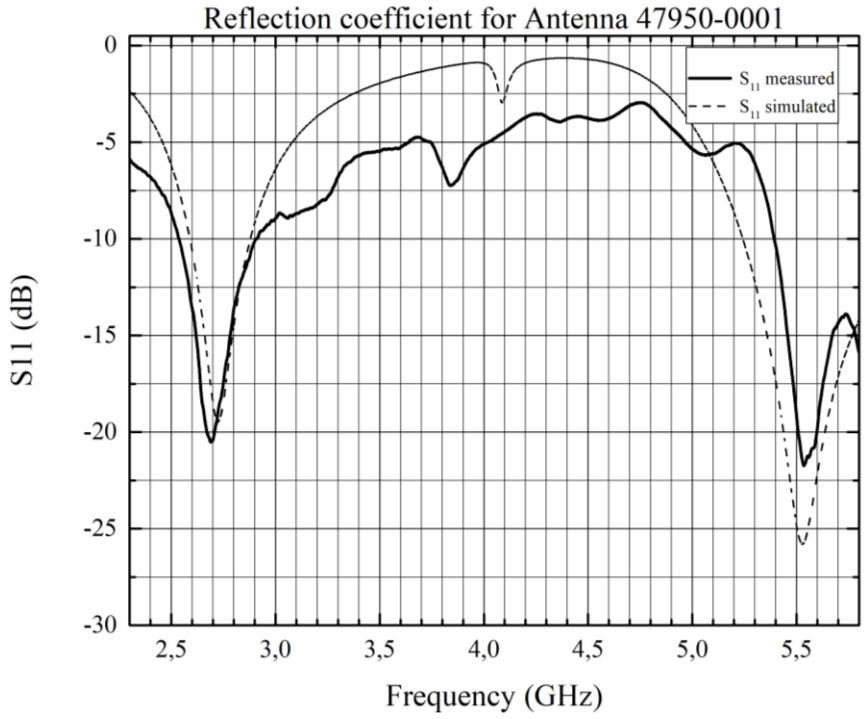

Figure 4-23. Reflection coefficient simulated and measured for the antenna 47950-0001 with a mesh refine

In the same way as the previous model, for a ε=3.5 and for an optimal mesh has been found in order to compare both responses.

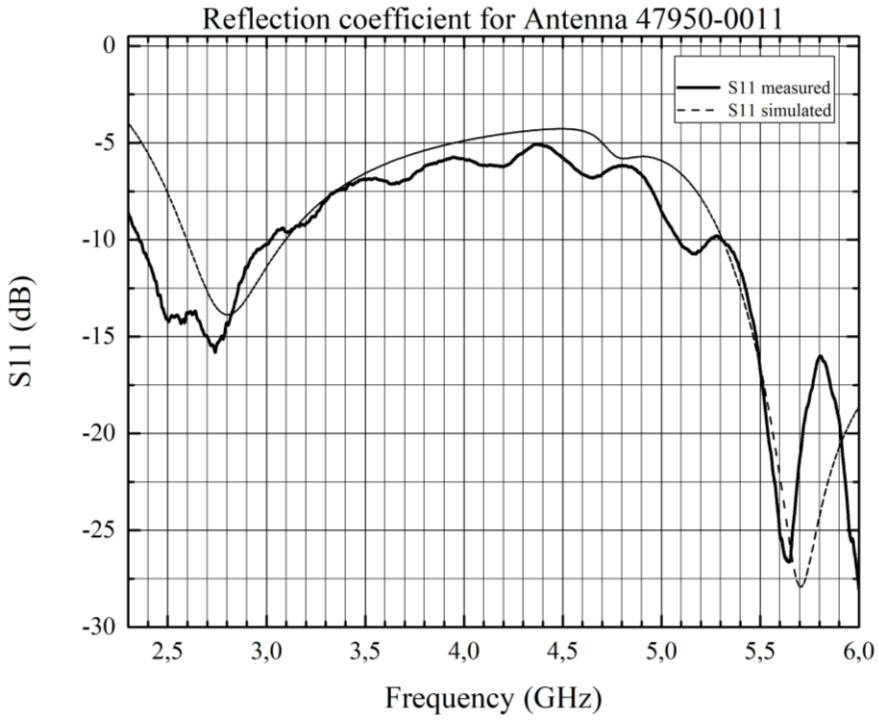

Figure 4-24. Reflection coefficient simulated and measured for the antenna 47950-00011

So, the maximum frequency adaptations obtained in the simulator CST is very similar at the reference measures obtained in the VNA E8357A [29] and verify a good design for the study.

Frequency of resonance	Antenna 47950-0001		Antenna 47950-0011	
	measured	simulated	measured	simulated
f_1 (GHz)	2.7	2.7	2.7	2.8
f_2 (GHz)	5.5	5.5	5.6	5.7

Table 4-5. Frequency resonances of the antenna 47950-0001 and 47950-0011

In Figure 4-25 and Figure 4-26 is represented the smith chart for defines the impedances. The antenna 47950-0001 at f_1=2.7 GHz have an impedance of 38.7+j0.33 Ω and at f_2=5.5 GHz of 26.8-j29.99 Ω. For the other antenna 47950-0011 at f_1=2.8 GHz is 39.6+j27.24 Ω and at f_2=5.7 GHz is 56.9-j13.37 Ω.

Note a capacitance behaviour for the high-band and an inductive behaviour for the low-band

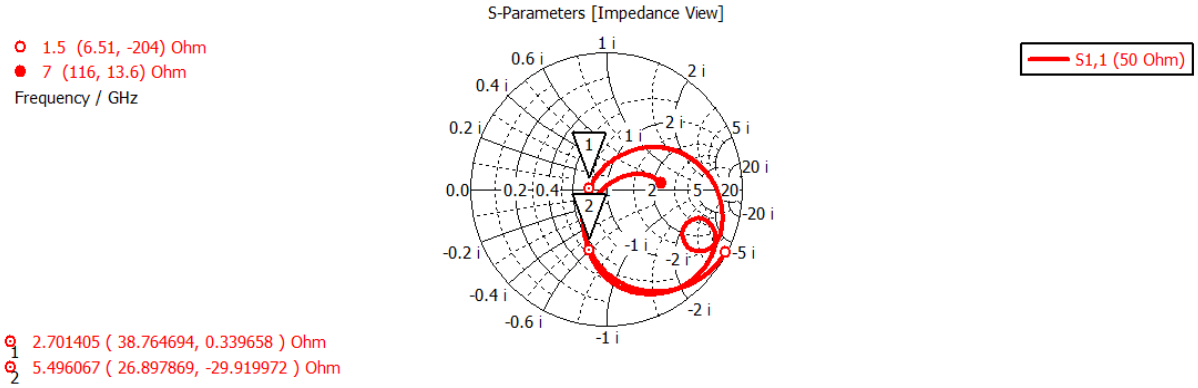

Figure 4-25. Smith chart of the antenna 47950-0001

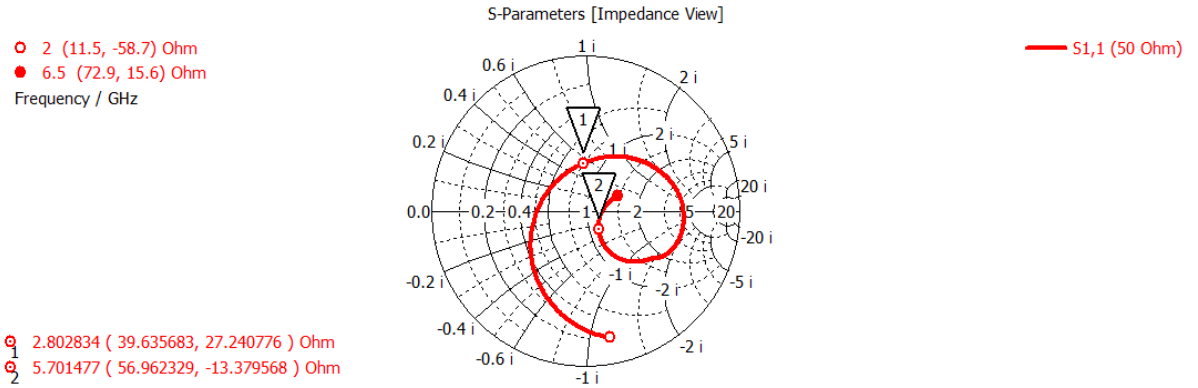

Figure 4-26. Smith chart of the antenna 47950-0011

For the frequencies of maximum adaptation indicates in the previous Table 4-5, is represented the current distribution for along of the structure for understand the behaviour of the antenna.

The current distribution plotted in Figure 4-27 for the antenna 47950-0001 shows maximum in the area between the gap of the two dipole sides due to the feed point. The distribution pattern of currents defines the side and the location of the frequency resonances. See although the two dipoles resonate for the first resonance at 2.7 GHz (Figure 4-27.a)) and second resonance at 5.5 GHz (Figure 4-27.b)), the current distribution patterns on the left and right sides are different.

a)

b)

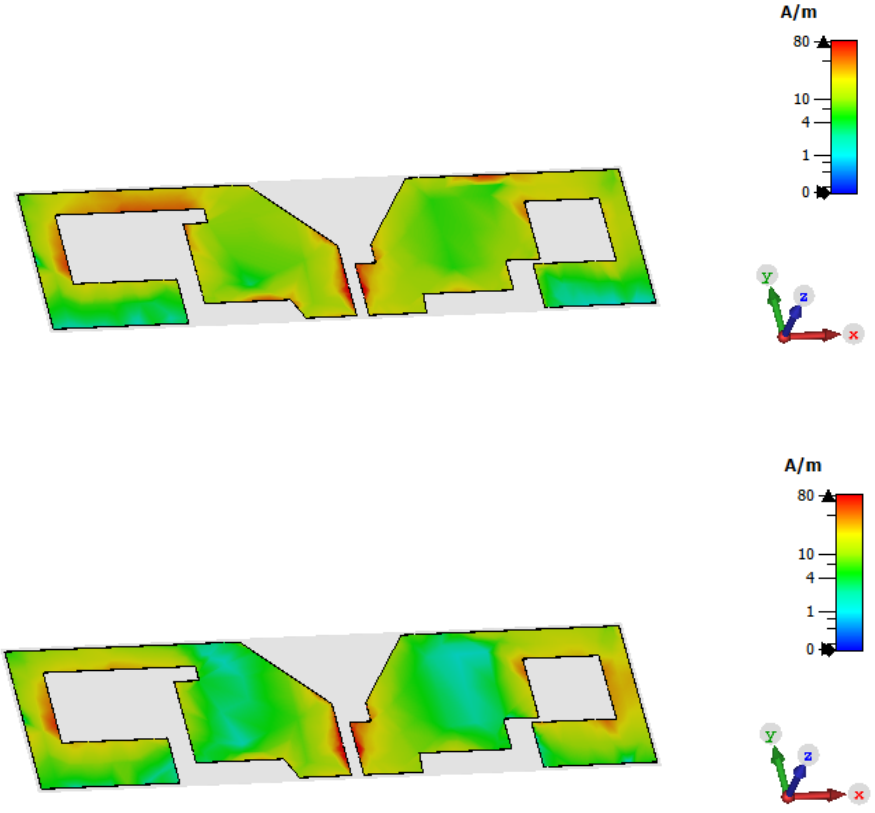

Figure 4-27. Current distributions for antenna 47950-0001 at 2.7 GHz a) and 5.5 GHz b).

For the current distributions in the antenna 47950-0011 (Figure 4-28), is observed the same high concentration at the location of the feed. The lower-band at 2.8 GHz and the high-band at 5.7 GHz have a similar distribution patterns as in the previous case in Figure 4-27, due to the similar geometry of the antenna even though the left and right sides are not symmetrical.

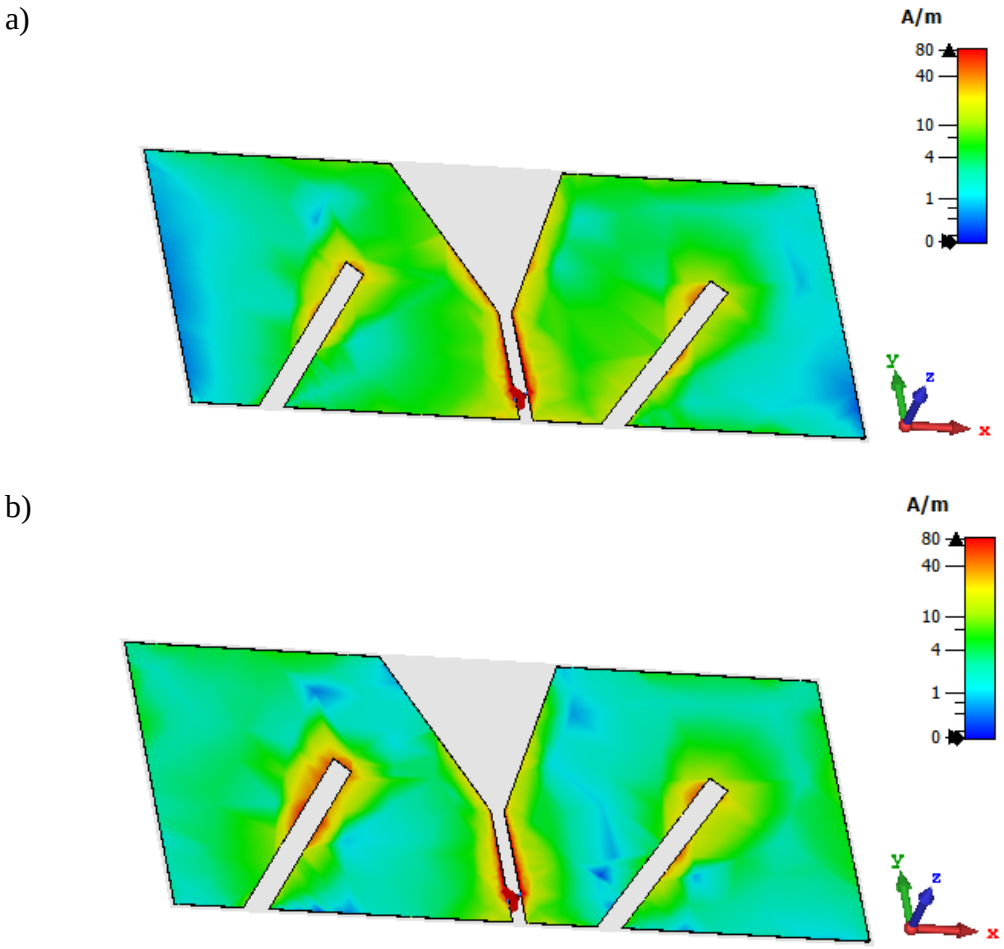

Figure 4-28. Current distributions for antenna 47950-0011 at 2.8 GHz a) and 5.7 GHz b).

The simulated density current distribution in both antennas show the relationship between the current distribution and the polygon shapes at a lower-band and high-band.

In Figure 4-29 is showed the radiation pattern of the antennas. It is a omnidirectional type of similar response and toroidal shape at the first resonance (see Figure 4-29.a) and Figure 4-29.c)) for the two antenna design. At the same time, at second resonances (see Figure 4-29.b) and Figure 4-29.d)) an omnidirectional behaviour is also observed with a deformation of the radiation pattern due to the effect of the low-band side which affects the field distribution.

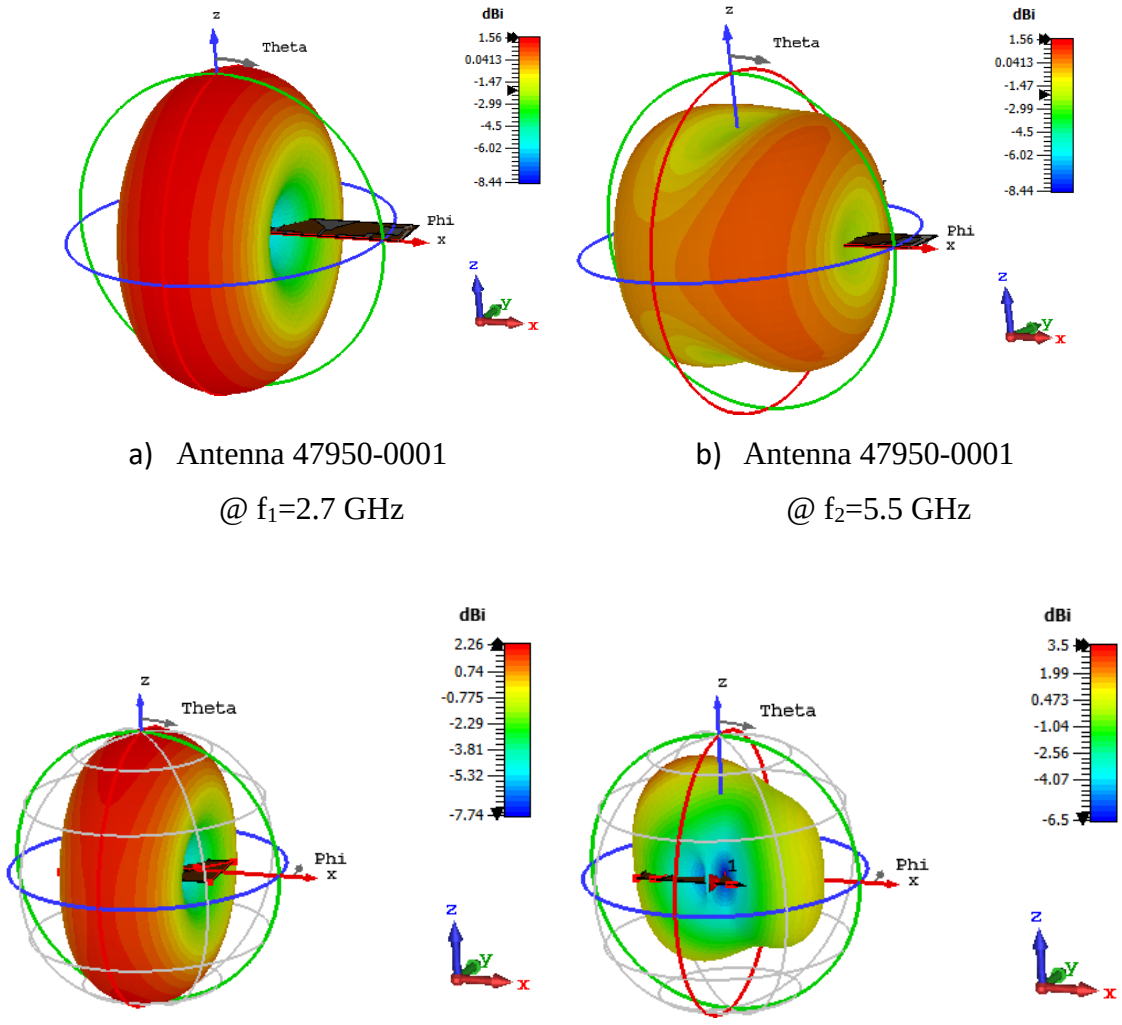

a) Antenna 47950-0001 @ f_1=2.7 GHz

b) Antenna 47950-0001 @ f_2=5.5 GHz

c) Antenna 47950-0011 @ f_1=2.7 GHz

d) Antenna 47950-0011 @ f_2=5.7 GHz

Figure 4-29. Radiation pattern for the antennas 47950-0001 and 47950-0011

From the radiation patterns is defined the gain at the low-band and high-band. The antenna 47950-0001 have a same maximum gain of 1.56 dBi for the both bands. But the antenna 47950-0011 in low-band is 2.26 dBi and in high-band is 3.5 dBi, probably due to the deformation, where there has been a change in the axis.

Finally, the electric field distribution of the dipoles antennas is illustrated at 2.4 GHz Figure 4-30:

a)

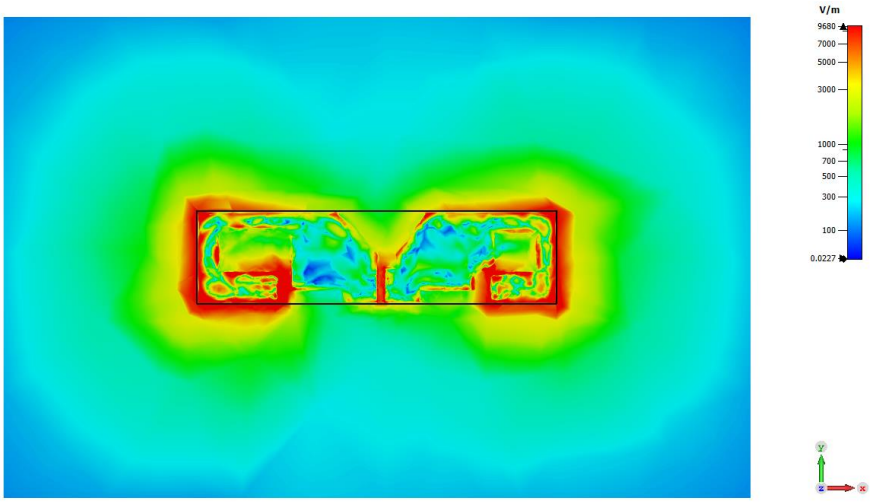

b)

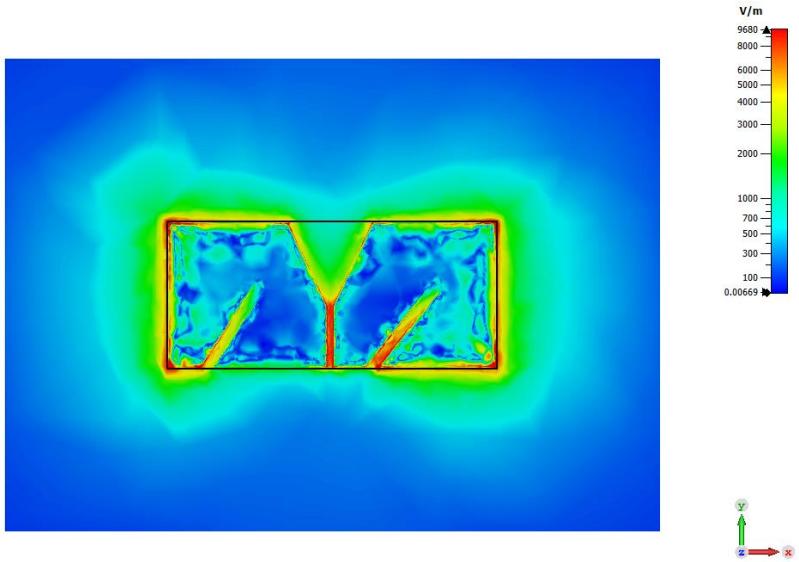

Figure 4-30. E-field distribution in YX axis at 2.4 GHz for the antenna 47950-0001 a) and 47950-0011 b)

In contrast with the inset-fed patch antenna (Figure 4-12), the E-field distribution of the dipole antennas show an inverted eight, being zero at the center of XY-axis and maximum at the sides.

These features results obtained are used to see the behaviour of the antenna such as the frequency of resonance, the geometry or electric field distribution in order to compare some differences in the application of the resonant cavity (chapter 5).

5 ENHANCED RF TRANSDUCER

The enhanced RF transducer is based on the application of a resonant cavity of Fabry-Perot composed by two metal layers, one up and one down, in the RF energy transducer proposed on a previous work [11] by the GAEMI group, which present the resonant cavity as an alternative to impedance matching to profit and increase the power at different frequencies up to 6 GHz. This RF energy transducer is composed by an antenna connected to a full-wave rectifier (bridge diode) and to a super-capacitance of 22 mF.

The resonant cavity of Fabry-Perot is applied it for the three antennas designed in chapter 4 and for a parametric study of the metal surfaces on CST Studio [18] with the purpose of see the effect in the enhanced RF transducer in function of the E-fields. Also, is tested for a first real set-up, where is measured the maximum voltage reached for a different size of metal surfaces.

5.1 MEASUREMENT FOR EXPERIMENTAL MEASUREMENT SET-UP

The enhanced RF transducer is tested with a Molex Combo antenna 47950-0001 to the study of a resonant cavity for the metallic surface sizes of 80x100 mm. 150x200 mm and 200x300 mm. These are made of FR4 with 35 µm of thickness.

Figure 5-1. Different metal surfaces of FR4 with 35 µm of thickness

The measuring set-up (see Figure 5-2) is composed for a 4-wire connection using the DC Power Analyzer N6705C [13] of two modules N6781A [14]. The 4-wire set-up ensures the accuracy of the measures due to the input impedance od the device can disturb the results.

a)

b)

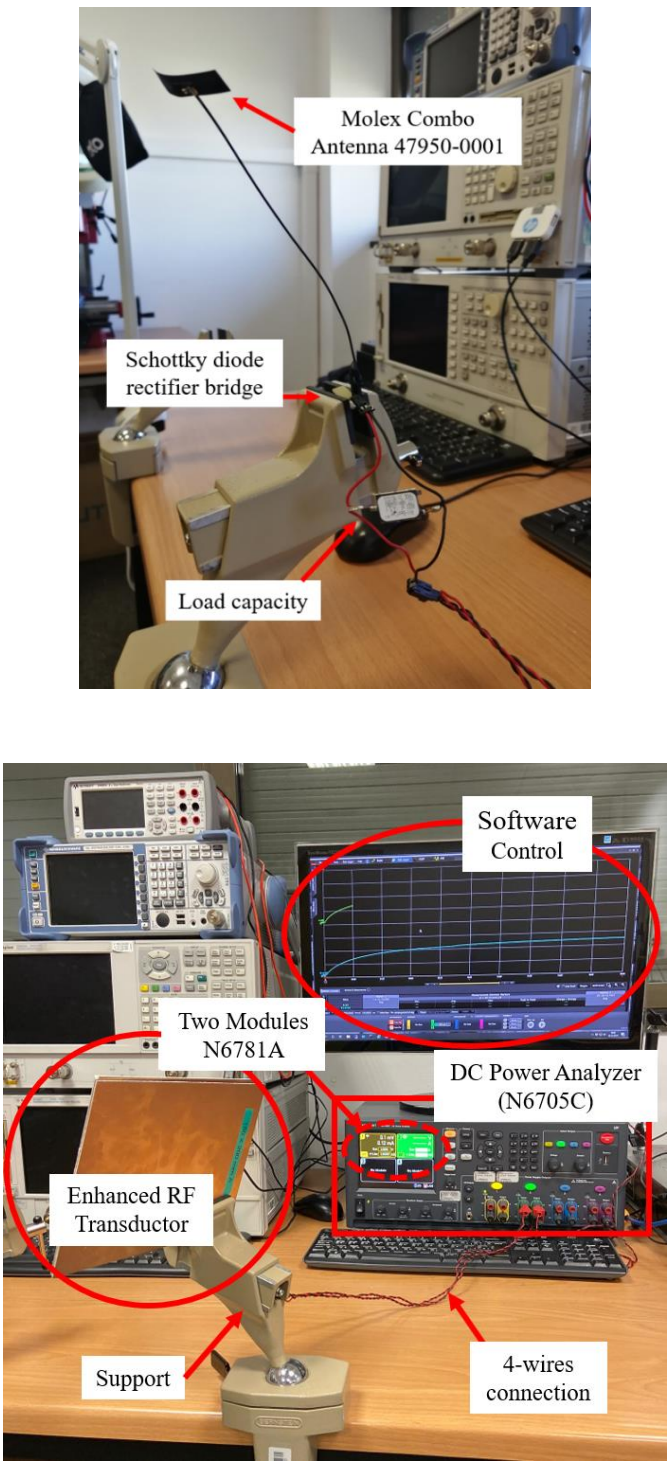

Figure 5-2. Experimental configuration with 4-wires connection between the RF transducer and DC Power Analyzer N6705C [13] by two modules N6781A [14]. a) The non-enhanced RF transducer is hold

by a support for orientate of the RF signal in direction of the router. b) The enhanced RF transducer is between two metal layers with the antenna by a support for orientate of the RF signal in direction of the router

In Figure 5-3 shows the main effect of the Fabry-Perot cavity achieving a maximum value around 1.5 V in fifteen minutes for the FR4 surface 200x300 mm, a voltage of 1.1 V for 150x200 mm surface and 1 V for 80x100 mm. These last results are similar despite of the different sizes, could be because of the similar length and width, i.e. on the 150x200 mm surface there is a sides differentiation of 20 mm and 50 mm for the 80x100 mm case compared to 200x300 mm which takes a difference of 100 mm. As longer is the side at the Wi-Fi router direction, it achieves a better result.

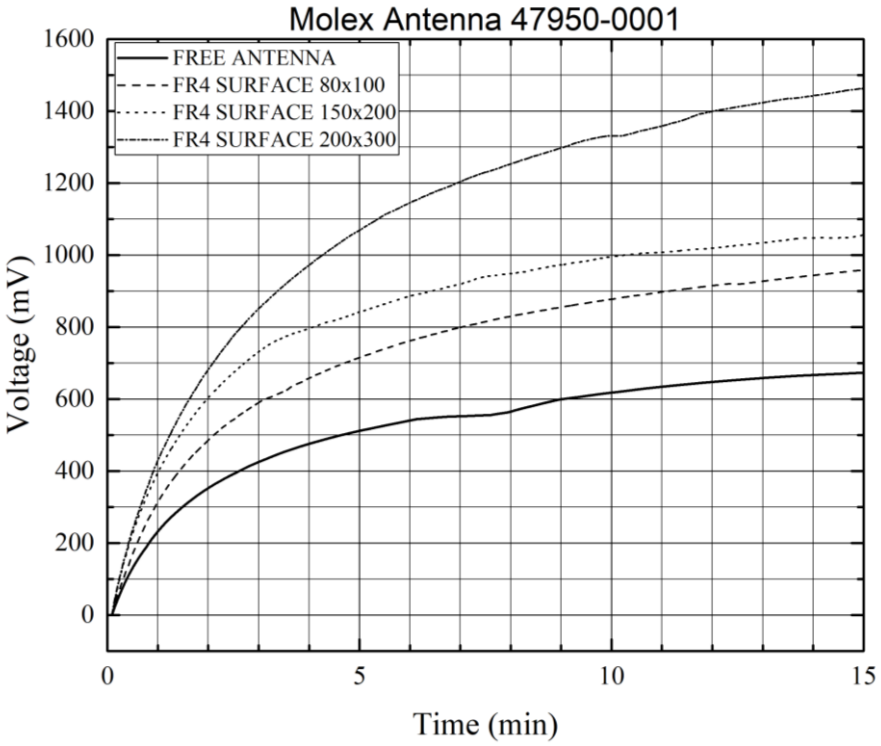

Figure 5-3. Output voltage of the enhanced RF transducer with a super-capacitance of 22 mF, for the Molex Combo antenna 47950-0001 and for different metallic surfaces by a measurement of 4-wire set up using a N6705C DC Power Analyzer [13] with two N6781A modules [14]

These results show the improvement for a dual-band antenna (Molex Combo 47950-0001[7]) with a super-capacitance of 22 mF, than the previous works in Figure 1-6, which is achieved 400 mV at 0.25 hours (15 minutes) for a super-capacitance of 8 mF. It changes of super-capacitance value affects in the charge time, but the improvement is due to the change of the antenna. The actual measures increase the non-enhanced RF transducer up to 3.5 times more.

Moreover, the measurement depends of the moment of the day. When there is most demand (at the morning) of the Wi-Fi, RF signals and voltage are increased. Almost 200 mV is the achieve value between the morning and afternoon measurements (see Figure 5-4).

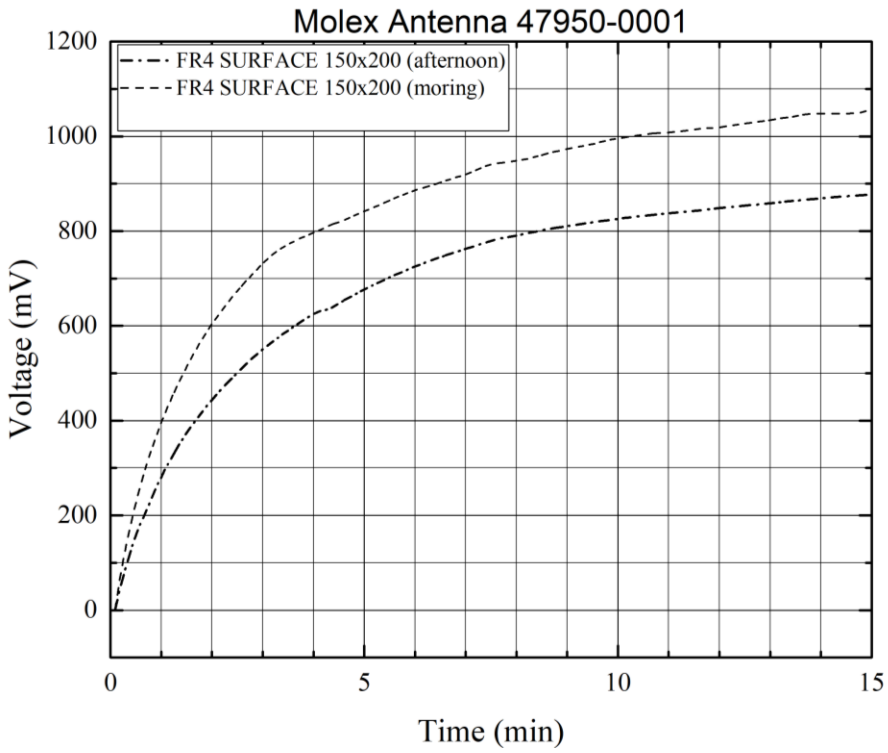

Figure 5-4. Output voltage of the enhanced RF transducer with a super-capacitance of 22 mF, for a Molex Combo antenna 47950-0001 and for different metallic surfaces by a measurement of 4-wire set up using a N6705C DC Power Analyzer [13] with two N6781A modules [14]

These results will be reference for the parametric study of the metallic surfaces on the CST studio [18] to understand the cavity effect.

5.2 SIMULATED BEHAVIOUR

The previous point 5.1 shows the response of the enhanced RF transducer when the metal surfaces is applied. In a simulation environment like CST Studio [18] is simulated the E-field distribution for see the resonant cavity effect with the application of the other parameters such as a gap between the resonant cavity through the E-field distribution at 2.4 GHz (see Annex 9.4), corresponded with the first resonance frequency of the far-field source. So, for the purpose of compare the behaviour is implemented the three different antennas designed of the chapter 4: the inset-fed patch antenna and the dipole antennas Combo 47950-0001 / 47950-0011.

Firstly, is designed a far-field source to work at 2.4/5 GHz (see Annex 9.4) as a Wi-Fi source and a resonant cavity between the antenna (Figure 5-5).

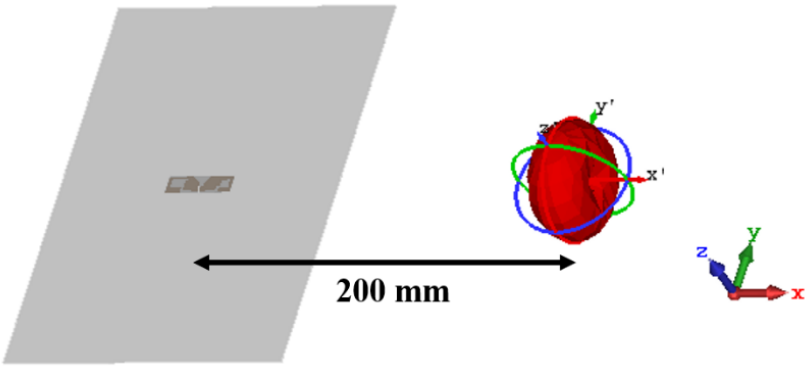

Figure 5-5. Schematic of enhanced RF transducer (left) for a far-field source (right) with a distance from the center of the antenna of 200 mm

5.2.1 Metal layers sizes

Taking account the sizes of the metallic surfaces in a measuring set-up (Figure 5-3) is simulated the E-field distribution when is applied the antenna between two metal surfaces of perfect electric conductor (PEC) for a gap of 1 mm (Figure 5-6) at 2.4 GHz. The gap is near to zero and equivalent to the measuring set-up, since the support applies a pressure in one side (see Figure 5-2.b)). Also, a null gap causes a short-circuit.

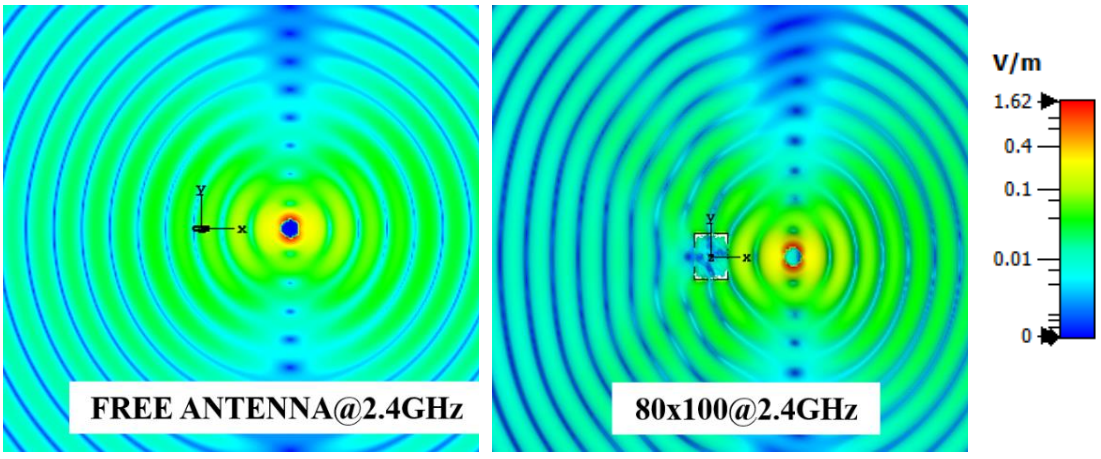

a) b)

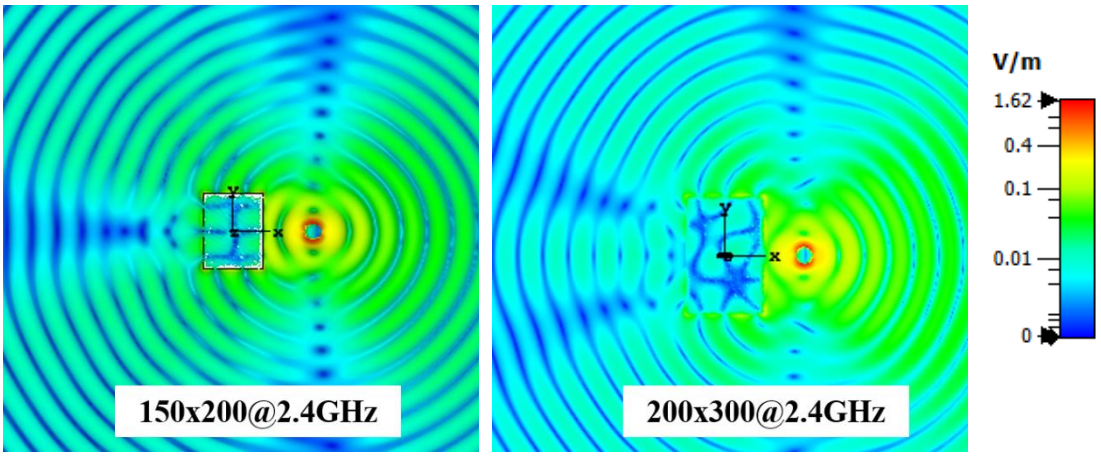

c) d)

Figure 5-6. E-field distribution at 2.4 GHz along XY-plane for Z=0 mm of the far-field source emitting in the left side. For the non-enhanced transducer a) and for the enhanced-transducer with gap=1 mm by Molex Combo 47950-0001 and metal layers of: 80x100 mm b), 150x200 mm c) and 200x300 mm d)

Look in Figure 5-6.b), c) and d), where is showed the absolute value of the electric field distribution in a plane perpendicular to the Z-plane at z=0 mm (between the metal surface). In the E-field distribution can be seen the field of the far-field source is able to penetrate between the metallic layers and reach the patch antenna along X-axis (right side). It can be compared with the Figure 5-6.a), where is illustrated the transducer without the cavity.

When the waves from the far-field arrives at the enhanced RF transducer, the resonant cavity produces multiple reflections out-of-phase of the RF signal from each other and that makes possible confine the RF power in the antenna enhancing the possibility to re-catch the reflected energy. See in Figure 5-6.b), c) and d) the blue area on the left part of the metallic layer, that could be interpreted by a lack of energy that mainly has been collected by the antenna resulting in an asymmetric emitter-transmitter behaviour.

For a resonant frequency of 5 GHz to the far-field source, the distribution of the E-field is along Y-axis, then the effect of the resonance cavity is visualized better due to the minimum values at the center of the far-field source along X-axis.

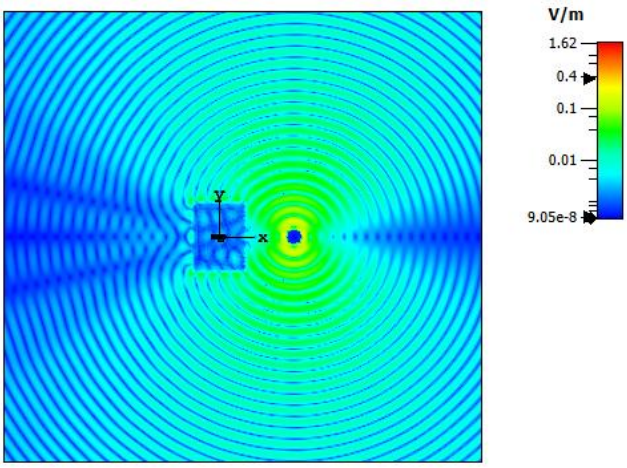

Figure 5-7. E-field distribution at 2.4 GHz along XY-plane for Z=0 mm of the far-field source emitting in the left side for the enhanced-transducer by Molex Combo 47950-0001 and metal layer 150x200 mm with gap=0.5 mm

On the other hand, in Figure 5-8 shows the E-field produced by the antenna, where the field outside the metallic layer is an evanescent wave that rapidly vanishes in the close vicinity. Noted the propagation of the antenna has changed with the metal surfaces, the field is distributed along the axes and not to the sides at X-axis as in Figure 4-30.a) without the resonant cavity.

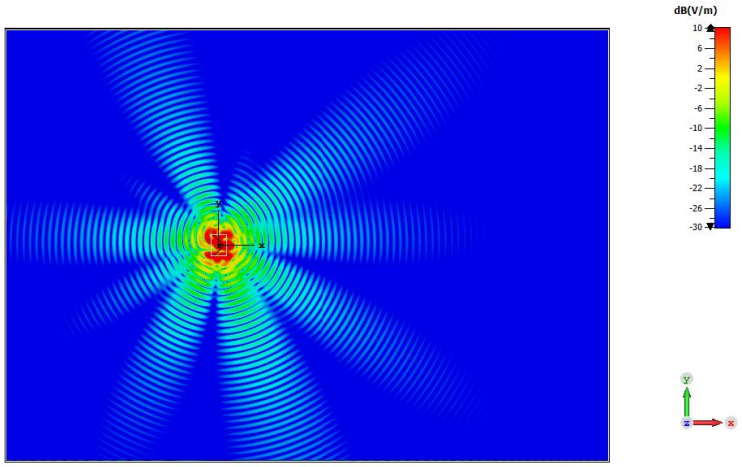

Figure 5-8. E-field distribution along XY-plane at Z=0 mm of the Molex Combo antenna 47950-0001 into the resonant cavity 150x200 mm at 2.4 GHz with a gap=1 mm

When the cavity effect is showed to different sizes, is then compared with the Molex Combo antenna 47950-0011 (Figure 5-9.a)) and the inset-fed patch antenna (Figure 5-9.b)). For this purpose, the residual area between the metal layer and the antenna must be the same because if the area is, for example bigger, the free metal area of the resonant cavity is decreased. Otherwise, for a little area the free metal area will be bigger.

So, the residual distances between the metal layer size of 150x200 mm and the Molex Combo antenna 47950-0001 corresponds with the expression:

$$W_{diff} = W_m - W_a = 150\ mm - 34.9\ mm = 115.1\ mm \quad (5.2\text{-}1)$$

$$L_{diff} = L_m - L_a = 200\ mm - 15.9\ mm = 191\ mm$$

Where, the W_m and L_m is the width and length of the metal layer dimensions and W_a and L_a for the antenna dimensions. Then, from (5.2-1) is calculated the equivalent distances.

$$W'_m = W_m + \left(W_{diff} - (W_m - W_a)\right)[mm] \quad (5.2\text{-}2)$$

$$L'_m = L_m + \left(L_{diff} - (L_m - L_a)\right)[mm]$$

The metal layers sizes for the Molex Combo antenna 47950-0011:

$$W'_m = 150 + \left(115.1 - (150 - 35.9)\right) = 151\ mm \quad (5.2\text{-}3)$$

$$L'_m = 200 + \left(191 - (200 - 15.9)\right) = 206.9\ mm$$

And for the inset-fed patch antenna:

$$W'_m = 150 + \left(115.1 - (150 - 52.82)\right) = 167.92\ mm \quad (5.2\text{-}4)$$

$$L'_m = 200 + \left(191 - (200 - 38.14)\right) = 229.14\ mm$$

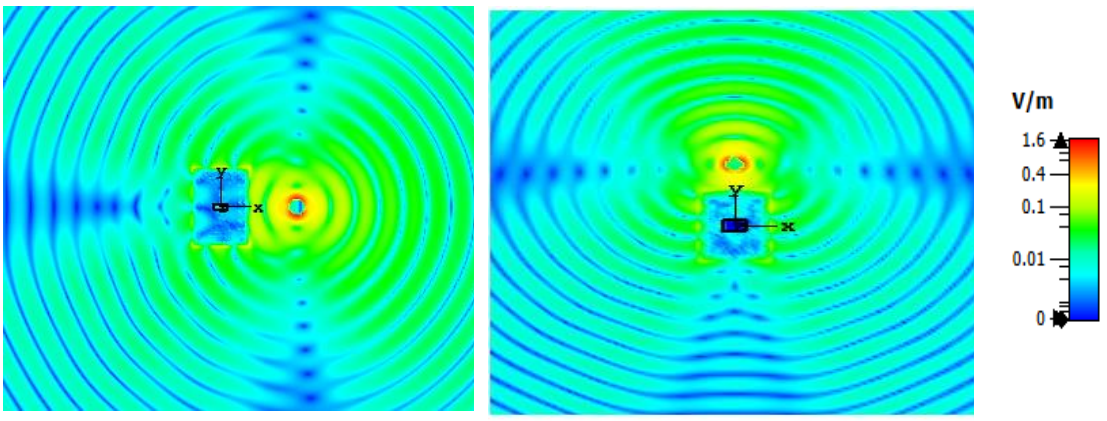

a) b)

Figure 5-9. E-field distribution at 2.4 GHz along XY-plane for Z=0 mm of the far-field source emitting in the left side for the enhanced-transducer by Molex Combo antenna 47950-0011 with a gap=1 mm and metal layers 151x206.9 mm a) and at top side for the inset-fed patch antenna with a gap=1 mm and metal layers 167.92x229.14 mm b)

Noted in Figure 5-9.b) that the far-field source is located at the top on the XY-axis due to the electric field distribution (see Figure 4-12). Then, for the same conditions the energy confine between the metal layers is improved in all cases (Figure 5-9), in comparation of the Molex Combo antenna 47950-0001 in Figure 5-6.c). The best case is for the inset-fed patch antenna (Figure 5-9.b)), due to the gain of 5.94 dBi is bigger than the Molex Combo 47950-0001 and 47950-0011 with gains of 1.56 dBi and 2.26 dBi, respectively.

5.2.2 Gap between the metal layers

The change of gap value implies the search and definition of the maximum distance where the resonant cavity stops working. At smallest distance (gap), the two metal surfaces operate as a capacitance and as a result the reflection coefficient S_{11} is deformed, in this case for a gap=20 mm from two peaks of adaptation to one and, decreasing return losses. In Figure 5-10, the capacitance effect starts to disappears from 100 mm of gap, when the reflection coefficient beginning to look like the original of the Figure 4-23.

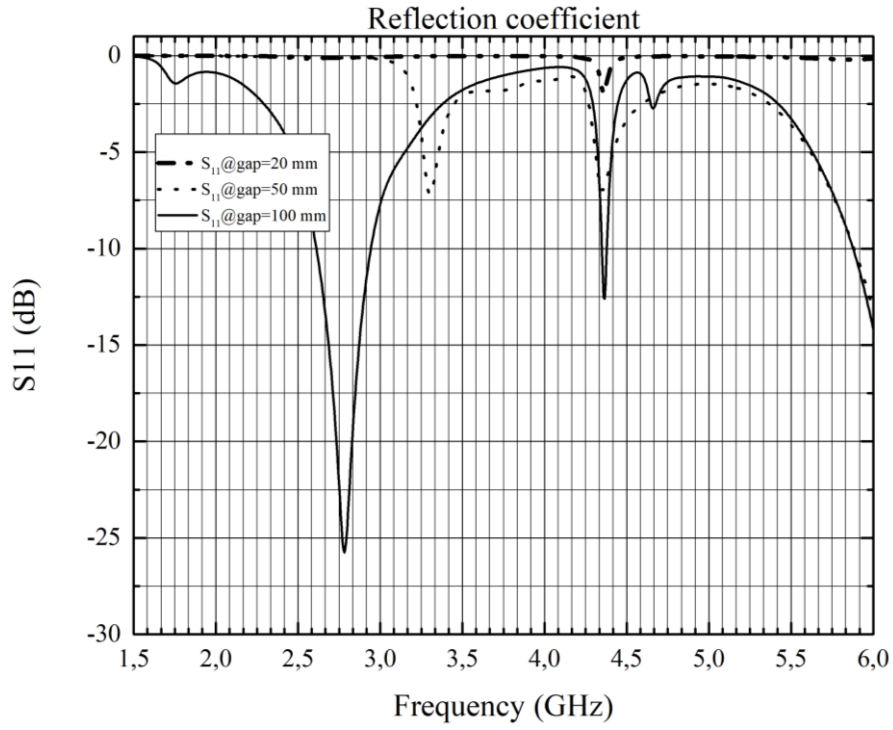

Figure 5-10. Reflection coefficient of the enhanced RF transducer for Molex Combo antenna 47950-0001 with a gap of 20 mm, 50 mm and 100 mm

For see better the effect of the gap into the metal layers, is simulated the response without the far-field at the simulate frequency of resonance 2.7 GHz defined in Table 4-5.

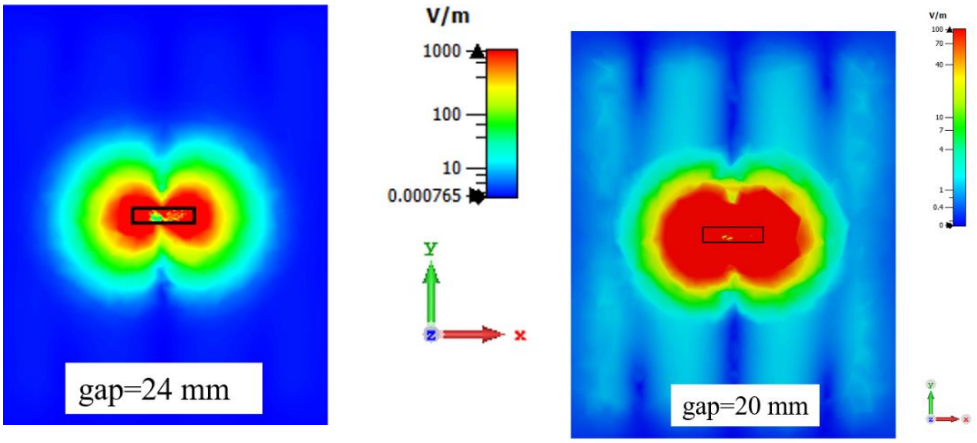

a) b)

Figure 5-11. E-field distribution at 2.7 GHz: of the enhanced RF transducer for Molex Combo 47950-0001, metal surface of 150x200 mm with a gap of 24 mm a) and 20 mm b)

The resonant cavity starts to collect energy near of 20 mm (Figure 5-11.b)), it can see in Figure 5-11.a) for a gap of 24 mm how it stops working, so the electric field distribution into the surfaces is less remarkable in comparation for a gap of 10 mm.

6 EFFICIENCY AND APPLICATION OF THE ENHANCED RF TRANSDUCER

6.1 EFFICIENCY

The results obtained in previous chapters about the maximum available ambient power in Figure 3-2 and the maximum voltage achieved in Figure 5-3 for a different metal surfaces to RF transducer, provides to estimate the efficiency of energy harvester system.

The efficiency is defined by the expression (6.1-2), where the RF power (P_{RF}) is the maximum available power at 5 GHz (see Figure 3-2) and the continuous power (P_{DC}) is corresponded with the output of the enhanced RF transducer, which is calculated for the super-capacitance of 22 mF used and the maximum voltage achieves for different metal surfaces size during 15 minutes (6.1-1).

$$P_{DC} = \frac{E}{\Delta t} = \frac{\frac{1}{2} \cdot C \cdot \Delta V^2}{\Delta t} \; [W] \tag{6.1-1}$$

$$\eta = \frac{P_{DC}}{P_{RF}} \cdot 100 \; [\%] \tag{6.1-2}$$

In Table 6-1 is calculated the efficiency of the experimental cases for the enhanced RF transducer using the experimental data depicted in (Figure 5-3):

Resonant cavity	P_{DC}	P_{RF}	η
FREE ANTENNA	6 µW	30 µW	20 %
80x100 mm	12.2 µW	30 µW	40.7 %
150x200 mm	14.8 µW	30 µW	49.3 %
200x300 mm	27.5 µW	30 µW	91.6 %

Table 6-1. Enhanced RF transducer efficiency for a different sizes of metal surfaces. The P_{DC} is measured at Δt=15 minutes for a super-capacitance of 22 mF. And the P_{RF} at 5 GHz

The values showed in the Table 6-1 even constituting a brought approach of the efficiency of the system indicate clear benefits in the utilization of the metallic cavities to enhance

the efficiency of the antennas as RF energy transducer. In any case, the calculated efficiencies improve the efficiency results reported in the literature, typically below 30 % [3].

6.2 COMBINATION OF THE ENHANCED TRANSDUCER WITH THE BQ25570 BASED ENERGY MANAGEMENT SYSTEM

The enhanced RF transducer uses to require an energy management system to complete the harvesting system. In order to show the viability of the proposed enhanced transducer, it has been used to feed a boost converter based in the integrated circuit (IC) BQ25570 [12] from Texas Instrument which is able to collect from the transducers μW delivering to mW pulses to the load. In the first approach, the evaluation module of the BQ25570 has been used to implement the energy management system (Figure 1-4).

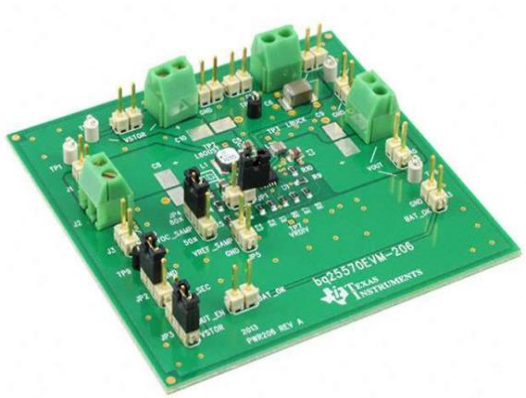

Figure 6-1. Evaluation module BQ25570EVM-206 by BQ25570 IC from Texas Instrument [12]

Is realized a first characterization of the enhanced RF transducer for a resonant cavity of 150x200 mm and for a Molex Combo antenna 47950-0001 (see Figure 6-2). In the graph is represented the input voltage of 330 mV required (see Annex 9.1) by the system and the maximum output voltage achieved of 1.8 V. This graph can be explained by three stages:

The first stage corresponds to a period of adaptation up to 4 hours, where the 1.1 V of input voltage provided of the enhanced RF transducer (Figure 5-3) is polarized to 330 mV required. After, the charging stage of the capacitor of 22 mF starts (high efficiency) until the last stage from 8 hours, which the amount charge is achieved a maximum output voltage of 1.8 V able to charge a battery.

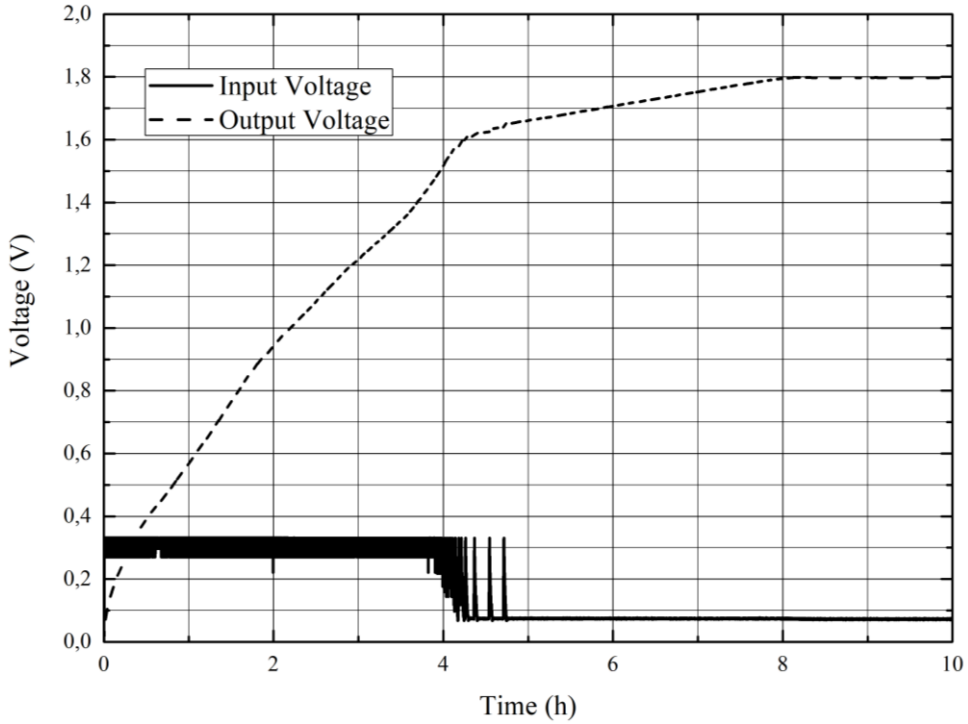

Figure 6-2. Output and input voltage of the step-up stage for the evaluation module BQ25570EVM-206 by BQ25570 IC from Texas Instrument [12]. The input voltage is provided of the enhanced RF transducer for a Molex Combo antenna 47950-0001 with a resonant cavity of 200x150 mm and a super-capacitance of 22 mF

The first stage corresponds to a period of adaptation up to 4 hours, where the 1.1 V of input voltage provided of the enhanced RF transducer (Figure 5-3) is polarized to 330 mV required. After, the charging stage of the capacitor of 22 mF starts (high efficiency) until the last stage from 8 hours, which the amount charge is achieved a maximum output voltage of 1.8 V able to charge a battery.

6.3 HARVEST-1 AND HARVEST-2

The first version of RF energy harvester system (based on the results obtained with the BQ25570 evaluation module) is the Harvest-1 developed by the GAEMI group of UAB. It is designed to rectify the signal from one Wi-Fi antenna and manage the rectified energy.

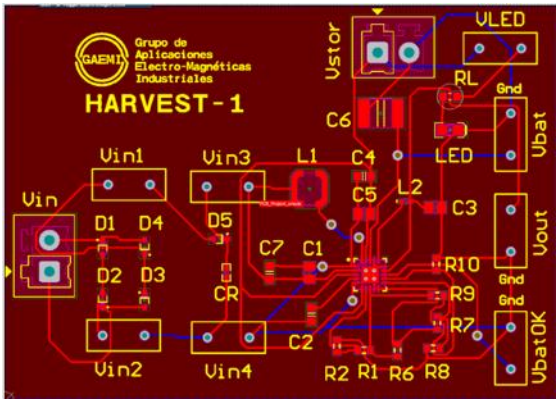

Figure 6-3. Layout of Harvest-1

The characterization of the enhanced RF transducer for a resonant cavity of 150x200 mm and for a Molex Combo antenna 47950-0001 (see Figure 6-4) is longer than the evaluation module (Figure 6-2) due to the components and the connections, but the maximum output voltage achieved of 1.9 V is slightly better.

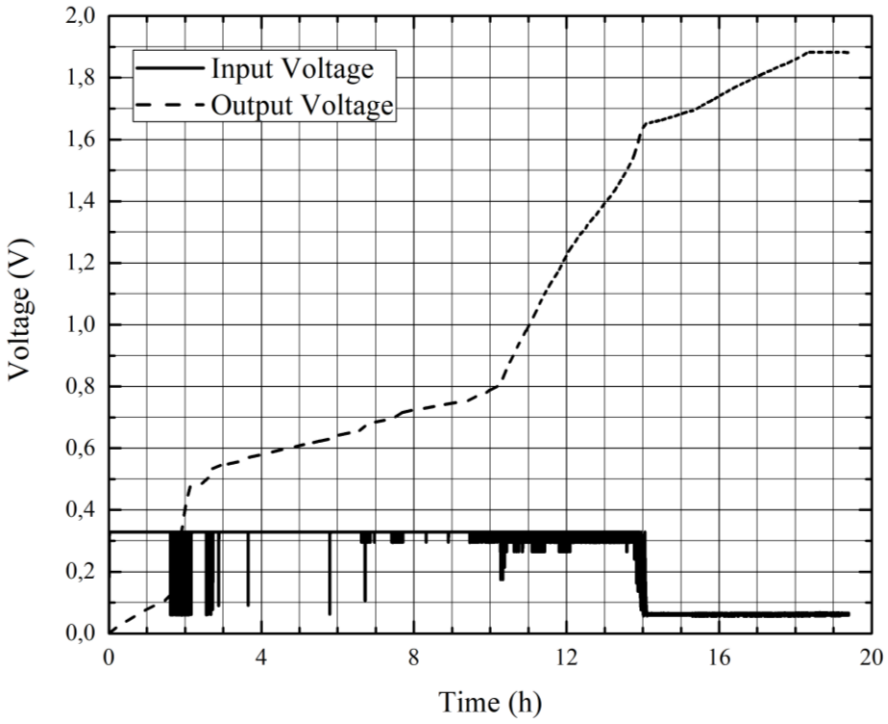

Figure 6-4. Output and input voltage of the step-up stage for the Harvest-1 by GAEMI group of UAB. The input voltage is provided of the enhanced RF transducer for a Molex Combo antenna 47950-0001 [7]with a resonant cavity of 200x150 mm and a super-capacitance of 22 mF

The first stage to reach the first stage of adaptation is up to 10 hours, which as the previous case, for 1.1 V of input voltage provided of the enhanced RF transducer (Figure 5-3) is polarized to 330 mV required. After, the charging stage of the capacitor of 22 mF starts

(high efficiency) until the last stage from 14 hours, which the amount charge is achieved a maximum output voltage of 1.9 V able to charge a battery.

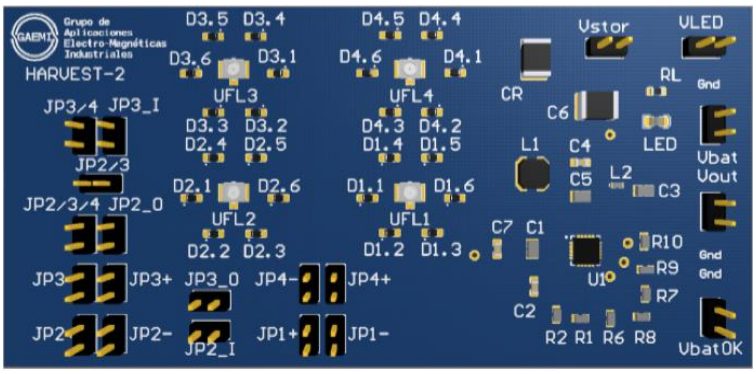

Figure 6-5. Layout of the Harvest-2

As a conclusion of these tests, it can be said that the utilization of the enhanced RF transducer allows the utilization of standard Wi-Fi antennas to feed energy management systems based on the BQ25570 IC. The GAEMI group have develop a PCB (Harvest-2, see Figure 6-5) that facilities to escalate the number of RF enhanced transducer up to 4 in combination with the BQ25570 IC based management system. The results with this new system are still in progress.

7 CONCLUSIONS AND FUTURE WORK

7.1 CONCLUSIONS

The present work has fulfilled the objectives determined in the beginning of the project with the purpose of realize a parametric analysis of the RF transducer performance in function of the two metal layers as a resonant cavity, one up and one down, with different size and the separation distance (gap) by means an analysis of confinement in RF antennas at Wi-Fi frequency band by full 3D electromagnetic simulation on CST Studio [18]. The aim of the project is to clarify the results obtained in a previous work [11] of the GAEMI group, which present the antenna confined in a resonant cavity as an alternative to impedance matching to profit and increase the power at different frequencies up to 6 GHz.

The amount of energy available in the working conditions for a dual-band antenna, Combo 47950-0001 from Molex, has been estimated from the frequential power density up to 6 GHz. The analysis of the power frequential density spectrum, shows that the important contributions to the environment RF energy comes from the 1.8 GHz and 2.4 GHz emissions. Just a few systems are actually radiating at 5GHz, being their contribution irrelevant to the overall amount of energy, even less important that the long-distance systems irradiating below 1 GHz (FM, AM base stations and GSM, for instance). The maximum value achieved is 30 μW and is used to reference magnitude to evaluate the efficiency of the RF energy transducer.

In the design of the inset-fed patch antenna or the antennas designed based on the description of two commercial dipoles antennas (Molex Combo antenna 47950-0001 / 47950-0011) has been difficult to fit of the reflexion coefficient in CST Studio with the experimental measures due to the search of an optimal mesh and good accuracy at the resonance frequencies in relation of reasonable simulation time, which has been fixed around of 15 minutes per simulation. Any variation in the mesh may be affect the accuracy, especially in the integral equation solver.

The voltage generated by the enhanced RF transducer has been measured for three different sizes of metal layer implemented by of FR4 with 35 μm of thickness: 80x100 mm, 150x200 mm and 200x300 mm. These experimental measurements show an improve of 3.5 times more of voltage with a resonant cavity size of 200x300 mm in comparation to the free antenna. Moreover, defines a significative results of efficiency in

each resonant cavity size from the maximum available power environment and the maximum achieved voltage and power due to the fact the typically efficiency of this RF harvesting systems is below 30 % [3]. The maximum efficiency for a resonant cavity size of 200x300 mm is 91.5 % and the minimum for the size 80x100 mm is 40.7 %, so without the metal layers for an efficiency of 20% the RF energy transducer cannot feed the energy management stage.

The mechanism of the transducer enhancements has been pointed out in the analysis of the electromagnetic field distributions at the antenna resonances. In a full 3D electromagnetic simulation, the behaviour of the electric field distribution of the far-field source at 2.4 GHz interacting with the enhanced RF transducer allows to see that the far-field is able to reach the antenna, producing multiple reflections out-of-phase of the RF signal from each other and that makes possible confine the RF power in the antenna enhancing the possibility to re-catch the reflected energy. Otherwise, the electric field by the antenna can see confined between the metal layers resulting in an asymmetric emitter-transmitter behaviour. The effect is incremented with the dimensions of the metallic layers. However, the effect of the cavity by means of the distance separation (gap) stop working to distances larger than 20 mm.

As a result of the simulation for the three antennas with the same size of resonant cavity, has been observed the possibility of enhanced the total amount of charge that the system is able to accumulate.

Finally, the enhanced RF transducer has been tested as feeding element of an energy management based on the BQ2570 IC from Texas Instruments The experimental data shows that the enhanced transducer is able to feed the manage energy system supplying enough energy to start up the system from a cold state to the high efficiency state in which it is able to charge a standard battery.

7.2 FUTURE WORK

The possibility to enhance the energy recollection performance of the antennas open a wide range of possibilities to extend the results obtained in this work. The reflection or resonance cavity could be adapted to other antennas geometries. The non-symmetric behaviour in the emission reception behaviour of the transducer constitute, by itself an interesting issue.

As immediate task, it would be interesting to combine several transducers with the Harvest-2 energy management system in other to scale up the amount of collected energy. In all the cases it will be interesting to combine the 3D full electromagnetic simulations with the rectifier circuits to develops a numerical tool suitable for optimization process.

8 REFERENCES

[1] Chong, G., Ramiah, H., Yin, J. et al. "Ambient RF energy harvesting system a review on integrated circuit design", Analog Integrated Circuits and Signal Processing 97:515, 2018

[2] CATRENE Working Group on Energy Autonomous System, "Energy autonomous systems: Future trends in devices, technology, and systems", 2009 [Online]. Available: https://pure.tue.nl/ws/portalfiles/portal/3255966/675451.pdf

[3] D. Pavone, A. Buonanno, M. D'Urso and F. D. Corte. "Design considerations for radio frequency energy harvesting devices", Progress in Electromagnetic Research B, vol. 45, pp. 19-35, 2012 [Online]. Available: http://www.jpier.org/PIERB/pierb45/02.12062901.pdf

[4] MA Abouzied, K. Ravichandran, E. Sánchez-Sinencio, "A fully integrated reconfigurable self-startup RF energy-harvesting system with storage capability", IEEE Journal of Solid-State Circuits. 2016; vol. 52(5), pp. 704-719.

[5] M. Piñuela, P. D. Mitcheson, and S. Lucyszyn. "Ambient RF energy harvesting in urban and semi-urban environments", IEEE Transactions on Microwave Theory and Techniques, vol. 61, no. 7, pp. 2715-2726, July 2013.

[6] B. White. "RF to DC Converter". Microwave and Wireless Engineering Program at Bradley University, 2016 [Online]. Available: http://ee.bradley.edu/projects/proj2016/rfdc/Final_Draft.pdf

[7] Molex. Datasheet: Combo Antenna 2.4GHz/5GHz model 47950-0001 [Online]. Available: https://www.molex.com/molex/products/datasheet.jsp?part=active/0479500001_ANTENNAS.xml&channel=Products&Lang=en-US

[8] Molex. Datasheet: Combo Antenna 2.4GHz/5GHz model 47950-0011 [Online]. Available: https://www.molex.com/molex/products/datasheet.jsp?part=active/0479500011_ANTENNAS.xml

[9] M. Cansiza, D. Altinelbc, G. Karabulut Kurt. "Efficiency in RF energy harvesting systems: A comprehensive review", Energy, vol. 174, pp. 292-309, May 2019.

[10] SKYWORKS. Datasheet: SMS7630-061: Surface Mount, 0201 Zero Bias Silicon Schottky Detector Diode [Online]. Available: http://www.skyworksinc.com/uploads/documents/SMS7630_061_201295H.pdf

[11] G.M. de Arriba, E. Coskuner, J.J. Garcia-Garcia, "Enhanced RF harvesting system by the utilization of resonant cavities", IEEE 2018 28th International Symposium on Power and Timing Modeling, Optimization and Simulation (PATMOS), 2018.

[12] National Instruments. Datasheet: BQ25570 nano boost charger and buck converter for energy harvester powered applications [Online]. Available: http://www.ti.com/lit/ds/symlink/bq25570.pdf

[13] Keysight. User Guide: N6705C DC Power Analyzer [Online]. Available: http://literature.cdn.keysight.com/litweb/pdf/N6705C-90901.pdf

[14] Keysight. Overview & Features: N6781A 2-Quadrant Source/Measure Units (SMUs) for Battery Drain Analysis, 20 V, ±1 A or 6 V, ±3 A, 20 W [Online]. Available: https://www.keysight.com/en/pd-1842316-pn-N6781A/2-quadrant-source-measure-unit-for-battery-drain-analysis-20-v-1-a-or-6-v-3-a-20-w?cc=CZ&lc=eng

[15] IEEE 802 standards [Online]. Available: https://ieeexplore.ieee.org/browse/standards/get-program/page/series?id=68

[16] "Wi-Fi Channels, Frequencies, Bands & Bandwidths", ElectronicsNotes. [Online]. Available: https://www.electronics-notes.com/articles/connectivity/wifi-ieee-802-11/channels-frequencies-bands-bandwidth.php

[17] IEEE Std 802.11n [Online]. Available: https://standards.ieee.org/content/dam/ieee-standards/standards/web/documents/interpretations/802.11n-2009_interp.pdf

[18] CST – Computer Simulation Technology [Online]. Available: https://www.3ds.com/products-services/simulia/products/cst-studio-suite/?utm_source=cst.com&utm_medium=301&utm_campaign=cst

[19] Rohde & Schwarz. User Guide: Spectrum Analyzer R&S – FSL [Online]. Available:

https://scdn.rohde-schwarz.com/ur/pws/dl_downloads/dl_common_library/dl_manuals/gb_1/f/sfl_1/FSL_OperatingManual_en_12.pdf

[20] European Telecommunication Standards Institute [Online]. Available: https://www.etsi.org/standards#Wireless%20Systems

[21] Wifi Analyzer Application [Online]. Available: http://wifianalyzer.mobi

[22] G.A. Deschamps, "Microwave antennas", Third USA symposium, 1953.

[23] J. Howell, "Microstrip antennas", IEEE International Symposium on Antennas and Propagation, 1972

[24] R. Munson, "Conformal microstrip antennas and phased arrays", IEEE Transactions on Antennas and Propagation, pp.64-77, 1974

[25] I.A. R.Garg, P.Bhartia, "Microstrip Antenna Design Handbook", Artech House, 2001

[26] C. A. Balanis, "Antenna Theory: Analysis and Design". John Wiley & Sons, New York, Edition 2005.

[27] D.M. Pozar, "Microstrip antennas", Proc. IEEE, 1992, vol. 80, (1), pp. 79–91, January 1992.

[28] LEICA. Datasheet: Microscope M80 [Online]. Available: https://downloads.leica-microsystems.com/Leica%20M80/Brochures/Leica_M50_M60_M80_TechData_EN.pdf

[29] KEYSIGHT TECHNOLOGIES. Datasheet: E8357A PNA Network Analyzer [Online]. Available: https://literature.cdn.keysight.com/litweb/pdf/5989-1077ENUS.pdf?id=450948

[30] KEYSIGHT TECHNOLOGIES. Datasheet: Cal Kit 85521A [Online]. Available: https://literature.cdn.keysight.com/litweb/pdf/85521-90001.pdf?id=2232814

9 ANNEXES

9.1 ELECTRICAL FEATURES OF THE ENERGY MANAGEMENT SYSTEM

Set of electrical characteristics of the energy management system at ambient temperature from the datasheet of the IC BQ25570[1] and guide user of the BQ25570EVM-206[2] module to obtain V_{OUT}=1.8 V and I_{OUT}=100 mV.

Parameters		Minimum	Maximum	Units
V_{IN} (CS)	Input voltage DC in V_{IN_DC}	330	600	mV
P_{IN} (CS)	Input power in V_{IN_DC}	0.0165	500	mW
I_{IN}	Input current in V_{IN_DC}	0.050	800	mA
Warm device (V_{BAT} > V_{BAT_UV})				
V_{IN}	Input voltage DC in V_{IN_DC}	80	5000	mV
P_{IN}	Input power in V_{IN_DC}	0.0016	4000	mW
I_{IN}	Input current in V_{IN_DC}	20	800	mA
Battery Management				
VBAT	Capacitor voltage of the internal load	2	5.5	V
VSTOR *	Capacitor voltage of the internal load	2	5.5	V
VBAT_OV	High voltage threshold in VBAT	2.2	5.5	V
VBAT_UV	Low voltage threshold in VBAT	1.9	2	V
Output V_{OUT}				
V_{OUT}	Output voltage in V_{OUT}	-	1.8	V
I_{OUT} **	Output current in V_{OUT}	-	100	mA

Table 9-1. Electrical features of the step-up stage

* Same voltages in VBAT and VSTOR due to the short-circuit. This configuration allows an improvement in the battery charging time for low powers in V_{OUT}.

** The output current is not constant. It is based on current pulses.

[1] National Instruments. Datasheet: [SLUSBH2F] BQ25570 nano power boost charger and buck converter for energy harvester powered applications. Available: http://www.ti.com/lit/ds/symlink/bq25570.pdf

[2] National Instruments. (SLUUAA7A) User's Guide for bq25570 Battery Charger Evaluation Module for Energy Harvesting. Available: http://www.ti.com/lit/ug/sluuaa7a/sluuaa7a.pdf

The output voltage must be connected to a rechargeable Li-on battery, thin film battery, supercapacitor or conventional capacitor, taking into account that it will be charged by means of current pulses up to 100 mA:

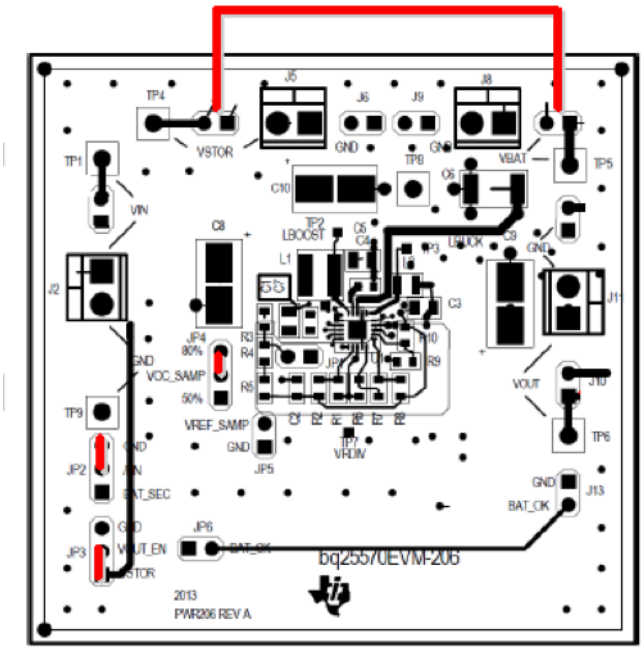

Figure 9-1. Short-circuit of the BQ25570EVM-206 between V_{BAT} and V_{STOR}

9.2 SCHEMATIC OF THE ENERGY MANAGEMENT SYSTEM

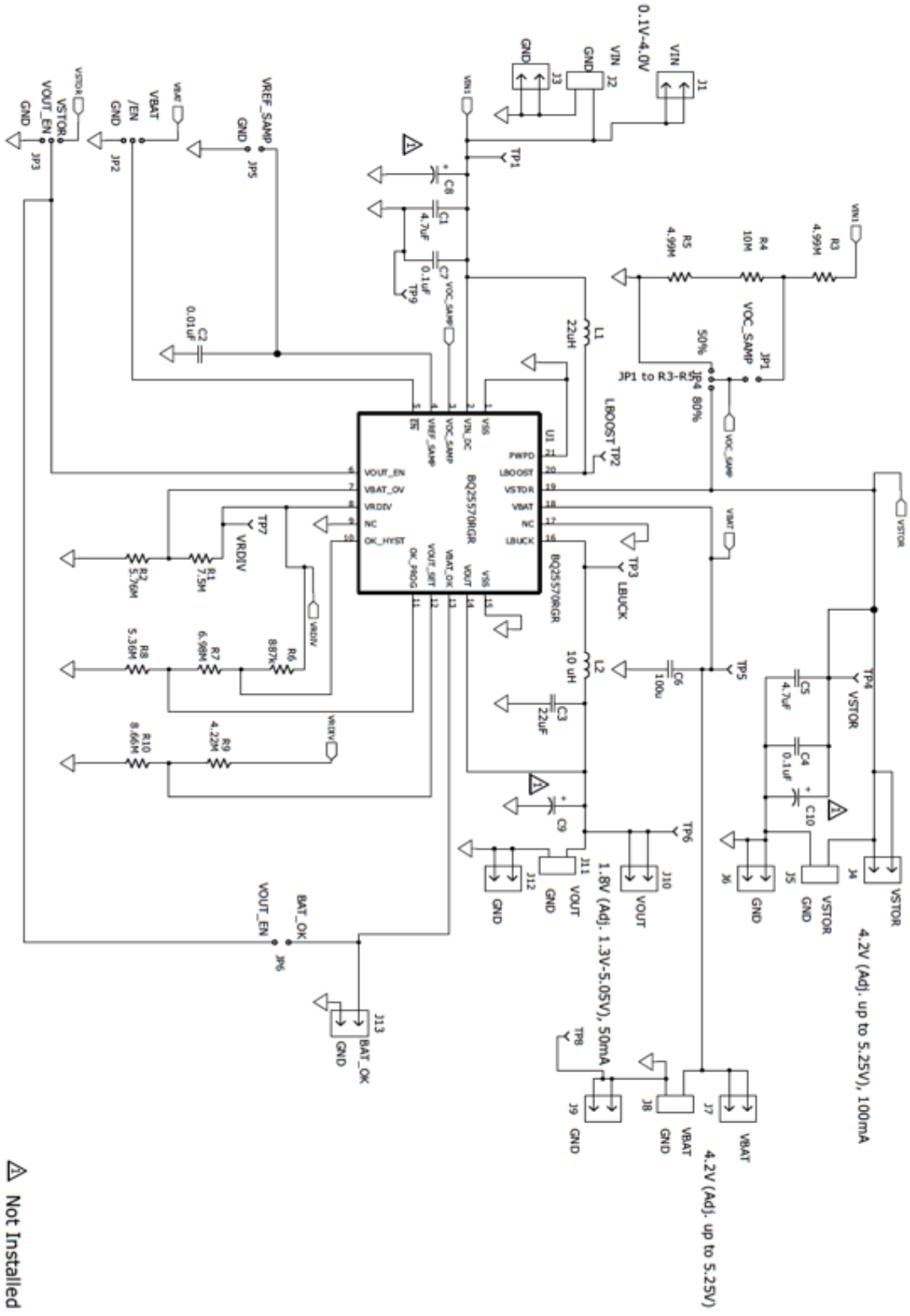

9.3 ELECTRONIC COMPONENTS OF THE ENERGY MANAGEMENT DEVICES

Count	RefDes	Value	Description	Size	Part Number	MFR
1	C1	4.7uF	Capacitor, Ceramic Chip, 6.3V, X7R, 10%	805	C0805C475K9RACTU	Kemet
1	C2**	0.01u**	Capacitor, Ceramic, 50V, X7R, 10%	0603	GRM188R71H103KA01D	Murata
1	C3	22uF	Capacitor, Ceramic Chip, 6.3V, X5R, 10%	805	JMK212BJ226MG-T	Taiyo Yuden
2	C4 C7	0.1uF	Capacitor, Ceramic Chip, 6.3V, X5R, 10%	603	06036D104KAT2A	AVX
1	C5	4.7uF	Capacitor, Ceramic Chip, 10V, X7R, 10%	805	LMK212B7475KG-T	Taiyo Yuden
1	C6	100uF	Capacitor, Ceramic Chip, 6.3V, X5R, 20%	1812	GRM43SR60J107ME20L	Murata
0	C8-10	DNP	Capacitor, Electrolytic, Snap Mt., wV	7343 (D)	n/a	n/a
9	J1 J3-4 J6-7 J9-10 J12-13	PEC02SAAN	Header, Male 2-pin, 100mil spacing,	0.100 inch x 2	PEC02SAAN	Sullins
4	J2 J5 J8 J11	ED555/2DS	Terminal Block, 2-pin, 6-A, 3.5mm	0.27 x 0.25 inch	ED555/2DS	OST
3	JP1 JP5 JP6	PEC02SAAN	Header, Male 2-pin, 100mil spacing,	0.100 inch x 2	PEC02SAAN	Sullins
3	JP2-4	PEC03SAAN	Header, Male 3-pin, 100mil spacing,	0.100 inch x 3	PEC03SAAN	Sullins
1	L1	22uH	Inductor, SMT, 0.65A, 360mΩ Inductor SMT, 0.36A, 410mΩ	4.0mmx4.0mmx1.80mm 3.8mmx3.8mmx1.65mm	LPS4018-223M 744031220	Coilcraft
1	L2	10 uH	Inductor, SMT, 1.4A, 216mΩ Inductor SMT, 250mA, 500mΩ Inductor SMT, 500mA, 390mΩ Inductor SMT, 500mA, 500mΩ	2.0mm x 2.5 mm 2.5mm x 2.0mm x 1.00mm 2.8mm x 2.8mm x 1.35mm 2.5mm x 2.0mm x 1.2mm	1239AS-H-100N 74479888310 744029100 74479889310	Toko Wurth Elektronik Wurth Elektronik Wurth Elektronik
1	R1	7.5M	Resistor, Chip, 1/16W, 1%	603	CRCW06037M50FKEA	Vishay Dale
1	R10	8.66M	Resistor, Chip, 1/16W, 1%	603	CRCW06038M66FKEA	Vishay Dale
1	R2	5.76M	Resistor, Chip, 1/16W, 1%	603	CRCW06035M76FKEA	Vishay Dale
2	R3 R5	4.99M	Resistor, Chip, 1/16W, 1%	603	CRCW06034M99FKEA	Vishay Dale
1	R4	10M	Resistor, Chip, 1/16W, 1%	603	CRCW060310M0FKEA	Vishay Dale
1	R6	887k	Resistor, Chip, 1/16W, 1%	603	CRCW0603887KFKEA	Vishay Dale
1	R7	6.98M	Resistor, Chip, 1/16W, 1%	603	CRCW06036M98FKEA	Vishay Dale
1	R8	5.36M	Resistor, Chip, 1/16W, 1%	603	CRCW06035M36FKEA	Vishay Dale
1	R9	4.22M	Resistor, Chip, 1/16W, 1%	603	CRCW06034M22FKEA	Vishay Dale
4	TP1 TP4-6	5002	Test Point, White, Thru Hole Color Keyed	0.100 x 0.100 inch	5002	Keystone
0	TP2-3 TP7	DNP	Test Point, 0.020 Hole	0.100 x 0.100 inch	STD	STD
2	TP8-9	5001	Test Point, Black, Thru Hole Color Keyed	0.100 x 0.100 inch	5001	Keystone
1	U1	BQ25570RGR	IC, Ultra Low Power Harvester Charger + Buck IC	VQFN	BQ25570RGR	TI
4			Shunt, 100-mil, Black	0.1	929950-00	3M
1	–		PCB, 2.5212 in x 2.6039 in		PWR206	Any

9.4 CST FAR-FIELD SOURCE FILE

```
// CST Far-field Source File
// Version:
3.0
// Data Type
Multipoles
// #Frequencies
2
//Position
0.2 0.0 0.0
//Start for theta (z'-axis)
0.0 0.0 1.0
//Start for phi (x'-axis)
1 0.0 0.0
// Radiated Power/Accepted Power/Stimulated Power [W,rms], Frequency [Hz]
-1
-1
-1
2.4e9

-1
-1
-1
5e9

// >> Total #multipoles
2

// >> n, m, Re(a), Im(a), Re(b), Im(b):
1  -1    1  0.0  0.0  0.0
1  +1    1  0.0  0.0  0.0

2

1  -1   -1  0.0  0.0  0.0
1  +1    1  0.0  0.0  0.0
```